Article:
Shi, Y-G, Zhang, R-R, Zhu, C-M et al. (6 more authors) (2021) Antimicrobial mechanism of alkyl gallates against Escherichia coli and Staphylococcus aureus and its combined effect with electrospun nanofibers on Chinese Taihu icefish preservation. Food Chemistry, 346. 128949. ISSN 0308-8146

https://doi.org/10.1016/j.foodchem.2020.128949

Elsevier Editorial System(tm) for Food Chemistry or its open access mirror
Manuscript Draft

Manuscript Number: FOODCHEM-D-20-06453

Title: Antimicrobial mechanism of non-antibiotic lipophilic gallic acid derivatives against Escherichia coli and Staphylococcus aureus and its combined effect with electrospun nanofibers on Chinese Taihu icefish (Neosalanx taihuensis Chen) preservation

Article Type: Research Article (max 7,500 words)

Keywords: alkyl gallates; antimicrobial mechanism; Escherichia coli; Staphylococcus aureus; electrospun nanofibers; reactive oxidative species; preservation

Corresponding Author: Professor Yugang Shi,

Corresponding Author's Institution:

First Author: Yugang Shi

Order of Authors: Yugang Shi; Run-run Zhang; Chen-min Zhu; Ming-feng Xu; Qing Gu; Rammile Ettelaie; Shan Lin; Yi-fan Wang; Xin-yi Leng

Abstract: A series of alkyl gallates were evaluated for the antibacterial activity against Escherichia coli and Staphylococcus aureus. The length of the alkyl chain plays a pivotal role in eliciting the antibacterial activity. Among them, octyl gallate (OG) exerted excellent inhibitory effect and potential mechanisms OG was fully elucidated, revealing a multiple bactericidal mechanism. The results demonstrated that OG function as a bactericide against both bacterial strains through damaging bacterial cell wall integrity, permeating into cells and then interacting with DNA, as well as disturbing the activity of the respiratory electron transport chain to induce a high-level toxic ROS (hydroxyl radicals) generation and up-regulation of the ROS genes. This research not only provides a more in-depth understanding of the interaction between OG and microorganisms but also highlights the great promise of using OG as a safe multi-functionalized food additive combined with the benefits of electrospun nanofibers for Chinese icefish preservation.

Dear Editors,

We would like to submit our manuscript entitled "Antimicrobial mechanism of non-antibiotic lipophilic gallic acid derivatives against *Escherichia coli* and *Staphylococcus aureus* and its combined effect with electrospun nanofibers on Chinese Taihu icefish (Neosalanx taihuensis Chen) preservation", which we wish to be considered for publication in *Food Chemistry*.

Phenolic acids are antioxidant compounds, which are widely used in the food and cosmetic industries because of their intriguing physiological functions. However, incorporating an alkyl chain into phenolic acids could modify their hydrophilic-lipophilic balance to generate amphiphiles molecules, called “phenolipids (PLs)”. Some phenolipids have shown stronger antibacterial activities against foodborne pathogens compared with the corresponding phenolic acid in that covalent modification of phenolic acids through lipophilization plays a dominant role in their capacities of passively permeating the cell membranes to reach their targets.

Herein, as shown in Figure 1,
(1) a series of alkyl gallates were synthesized through enzymatical reactions and evaluated for the antibacterial activity against *Escherichia coli* and *Staphylococcus aureus*. The length of the alkyl chain plays a pivotal role in eliciting the antibacterial activity.

(2) Among them, octyl gallate (OG) exerted excellent inhibitory effect and potential mechanisms OG was fully elucidated. The results show that OG damages the membrane and permeates into cells and then interacts with DNA. OG could further disturb the activity of the respiratory electron transport chain (ETC) to induce a high-level toxic ROS (hydroxyl radicals) generation and up-regulation of the ROS genes. These results illustrated OG has multiple mechanisms of bactericidal action, ultimately leading to cell death.

(3) Moreover, the ultra-efficient and safe antibacterial system was constructed using OG encapsulated with nanofibers by electrospinning and its synergetic sterilization effect was also ascertained on the microbial load of Chinese Taihu icefish (Neosalanx taihuensis Chen).

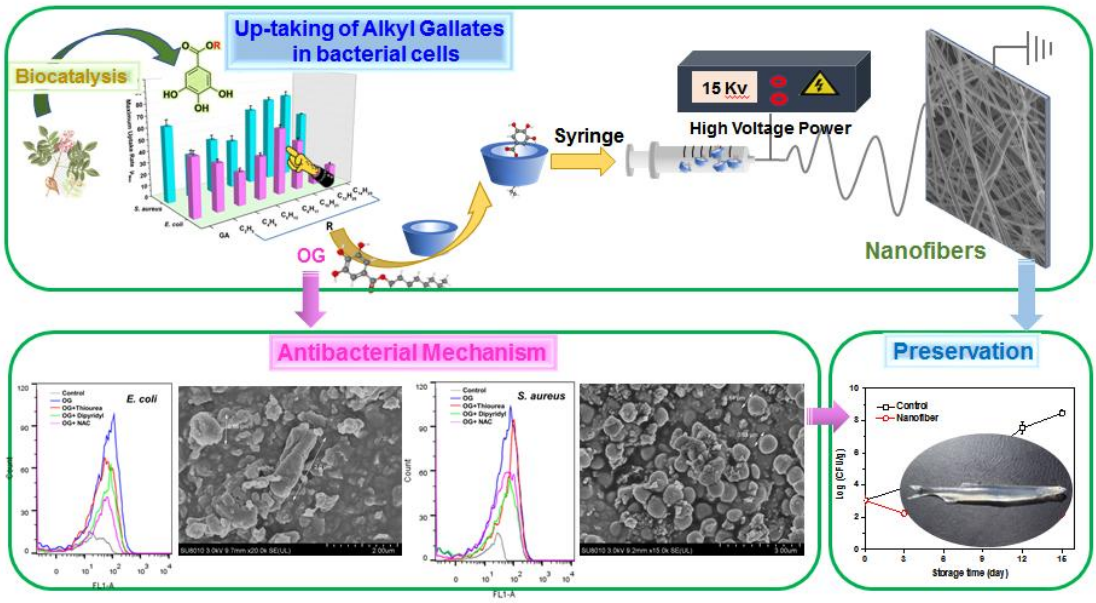

Figure 1. Schematic of the main aims of this present work

Thank you so much for your consideration and time.

Sincerely yours,

Dr. Yugang Shi

Corresponding author:
Yugang Shi, School of Food Science and Biotechnology, Zhejiang Gongshang University, Zhejiang Province key lab of Food Safety, HangZhou 310035, China
yugangshi@zjgsu.edu.cn
Phone number: +86-0571-28008927
Fax number: +86 88056656

Highlights:

- Incorporation of aliphatic molecules into GA to ameliorate antibacterial activities
- Antibacterial activities of alkyl gallates were evaluated
- The mode of action of octyl gallate was systemically investigated
- Nanofibers with octyl gallate have unique superiorities for icefish preservation

Submit online to *Food Chemistry*

Antimicrobial mechanism of non-antibiotic lipophilic gallic acid derivatives against *Escherichia coli* and *Staphylococcus aureus* and its combined effect with electrospun nanofibers on Chinese Taihu icefish (*Neosalanx taihuensis* Chen) preservation

Yu-gang Shi*[a, b], Run-run Zhang [a], Chen-min Zhu [a], Ming-feng Xu [c], Qing Gu [a, b], Rammile Ettelaie [d], Shan Lin [a], Yi-fan Wang [a], Xin-yi Leng [a]

[a]*School of Food Science and Biotechnology, Zhejiang Gongshang University, Hangzhou, Zhejiang 310035, China*

[b]*Key Laboratory for Food Microbial Technology of Zhejiang Province, Zhejiang Gongshang University, Hangzhou, Zhejiang 310035, China*

[c] *Key Laboratory for Quality and Safety of Agricultural Products of Hangzhou ,College of Life and Environmental Sciences, Hangzhou Normal University, Hangzhou 311121, China*

[d]*School of Food Science and Nutrition, University of Leeds, Leeds, LS2 9JT, UK*

Corresponding Author:

Yu-gang Shi

School of Food Science and Biotechnology, Zhejiang Gongshang University, Xiasha University Town, Xuezheng Str. 18, Hangzhou 310018, China

Tel.: 86–0571–28008927

Email: yugangshi@zjgsu.edu.cn

ABSTRACT

A series of alkyl gallates were evaluated for the antibacterial activity against *Escherichia coli* and *Staphylococcus aureus*. The length of the alkyl chain plays a pivotal role in eliciting the antibacterial activity. Among them, octyl gallate (OG) exerted excellent inhibitory effect and potential mechanisms OG was fully elucidated, revealing a multiple bactericidal mechanism. The results demonstrated that OG function as a bactericide against both bacterial strains through damaging bacterial cell wall integrity, permeating into cells and then interacting with DNA, as well as disturbing the activity of the respiratory electron transport chain to induce a high-level toxic ROS (hydroxyl radicals) generation and up-regulation of the ROS genes. This research not only provides a more in-depth understanding of the interaction between OG and microorganisms but also highlights the great promise of using OG as a safe multi-functionalized food additive combined with the benefits of electrospun nanofibers for Chinese icefish preservation.

Keywords: alkyl gallates, antimicrobial mechanism, *Escherichia coli*, *Staphylococcus aureus*, electrospun nanofibers, reactive oxidative species, preservation

1. Introduction

Due to the diverse requirements in the marketing of food products, the use of chemical additives in food, such as antioxidant and antimicrobial agents, has still gained a growing level of importance to preserve flavor and enhance its texture or appearance, or for other technological functions. Many studies have shown that microorganisms are the primary factor in the degeneration of food during transportation and storage (Li, Cui, Bai, Zhao, & Li, 2016), which leads to significant losses to the food industry. For instance, most fish species highly degrade as a result of microbial spoilage from surface bacteria. Moreover, diseases caused by foodborne microorganisms in food remain one of the greatest threats to both public health and the food industry, especially, in developing countries like China. It was reported that 140,101 foodborne diseases and 1,427 deaths had been recorded from 2001 to 2010 in China (Luo, Li, Liu, & Tan, 2017). As a global foodborne pathogenic bacteria, *Staphylococcus aureus* (*S. aureus*) can invade the body and cause a wide range of infections, including food poisoning. Food products can induce *S. aureus* growth and activate staphylococcal enterotoxin which is responsible for gastrointestinal illness. *Escherichia coli* (*E. coli*) is a common cause of food poisoning which is considered the world's third most significant cause of diseases such as severe gastroenteritis, hemorrhagic colitis, and the life-threatening hemolytic-uremic syndrome. The prevalence of antimicrobial resistance among foodborne pathogens has increased during recent decades. For instance, a significant antibiotic-resistant had been noticed in Shiga toxin-producing *E. coli* O157: H7 (Chirila et al., 2017). This requires new non-antibiotic substances to inhibit bacteria, bringing safety and security to the food industry. Natural products are the best choice, and their excellent antibacterial and antioxidant effects are in line with people's needs.

Lately, phenolic compounds (phenolic acids, in particular) have obtained an increasing interest in the food industry stemming from their potential bioactive properties. In addition, plant phenolics and extracts rich in such substances can be excellent inhibitors of many foodborne pathogenic and spoilage bacteria activities. In our continuing search for antimicrobial agents as food preservatives (Shi et al., 2017; 2018; 2019), incorporating an alkyl chain into a carboxyl group of phenolic acids could modify their hydrophilic-lipophilic balance to generate amphiphiles molecules, called "phenolipids (PLs)". Some phenolipids have shown stronger antibacterial activities against foodborne pathogens compared with the corresponding phenolic acid in that covalent modification of phenolic acids through lipophilization plays a dominant role in their capacity of passively permeating the cell membranes to reach their targets. Recently, a series of alkyl ferulates have been prepared and their biological activities were compared by us. Interestingly, it has been found that as the length of the alkyl chain extends, the antibacterial activity begins to rise, and a point is soon

reached beyond which activity disappears (the so-called 'cut-off' phenomenon). Among them, hexyl ferulate (FAC6) was most effective against *E. coli*, *Listeria monocytogenes* (*L. monocytogenes*) and *S. aureus* (Shi et al., 2017; 2018; 2019). Similarly, butanol ferulate (FAC4) is more active than ferulic acid and ethyl ferulate (FAC2), as well as the other alkyl ferulic esters, to effectively protect the PC12 cells against oxidative stress through reducing ROS formation and inhibiting $A\beta_{1-42}$ aggregation (Shi et al., 2020). These results supported the fact that the length of the alkyl group considerably influenced their biological activities to a large extent.

It has been reported that the mechanism of action of gallic acid (GA), a hydroxybenzoic acid, is similar as that of ferulic acid, a hydroxycinnamic acid, when assessed on *E. coli*, *Pseudomonas aeruginos*a, *S. aureus*, and *L. monocytogenes* (Borges, Ferreira, Saavedra, & Simões, 2013). Moreover, GA is a widely occurring metabolite in the plant kingdom and well known for its antioxidant, antibacterial, anti-inflammatory, anticarcinogenic, antiviral and analgesic properties (Giftson, & Jayanthi, 2008; Kang et al., 2008; Kim et al., 2006). Also, phenolipids based on GA, especially alkyl gallates, exhibited more favorable properties, and in many cases, these effects were even stronger than those observed for GA itself. GA and its alkyl esters, as phenolic antioxidants, are widely found in wine and green tea (Butt, & Sultan, 2009). To date, in addition to their antioxidant activity, alkyl gallates have been reported to exhibit various other biological activities. For instance, GA-based phenolipids with eight or more carbon atoms in the side-chain were more efficient than GA in antimicrobial (Kubo et al., 2001; 2002; 2003; 2004) and antitumor activity, and the chain lengths of alkyl gallates significantly affected their antibacterial activities. Notably, in comparison to other alkyl gallate esters, octyl gallate (OG), exhibits an outstanding antibacterial effect against *Salmonella choleraesius*, *Bacillus subtilis*, *Saccharomyces cerevisiae*, *Zygosaccharomyces bailii*, *Monilia albicans* and *Aspergillus Niger* (Kubo, 2002; 2003; 2004). Moreover, OG has been approved for use as antioxidant additives in the food and pharmaceutical industries because of significantly low toxicity both in vitro and in vivo (Sivasankaran, Vikraman, Thomas, & Kumar, 2016). However, to the best of our knowledge, the intrinsically antibacterial mechanism of alkyl gallates against foodborne bacteria on the one hand, the role of the hydrophobic portion on the other, has hitherto remained poorly understood and wildly debated. Concurrently, few studies have been conducted on whether alkyl gallates have the potential to be considered as multi-functionalized food preservatives that satisfy quality maintenance and safety drivers for consumers. Hence, their further evaluation was undertaken to gain comprehensive insights into their bactericidal action. More importantly, an agent with the dual function as an antioxidant (generally, in preventing food lipid oxidation) and antimicrobial (preventing the growth of pathogenic and

spoilage bacteria) would provide us more promising options in the food industry with minimizing the total amount of additives used in foods. Furthermore, electrospun nanofibers incorporated with antimicrobial agents can not only drive the durable release of bioactive agents from nanofibers to the food surface but also amplify notable synergistic antibacterial effects on a wide range of microorganisms(Lou, Osemwegie, & Ramkumar, 2012). As such, it would be more meaningful for the incorporation of electrospun nanofibers with the efficient antibacterial agents.

In this paper, we examined the antibacterial activity of alkyl gallates against both foodborne pathogenic Gram-negative (G–) *E. coli* and Gram-positive (G+) *S. aureus* as model microorganisms. The antibacterial experiments reveal that OG exhibits extensive bacteriostatic and bactericidal ability against both strains. Moreover, in addition to the role of the hydrophobic alkyl moiety of gallates, the antibacterial mechanism of OG against tested bacterial species has been predominantly characterized through a series of methods including the evaluation of cellular membrane permeability and integrity, the alterations in the membrane fatty acids composition and bacterial morphology, intracellular damage caused by the participation of reactive oxygen species (ROS), as well as the interaction between OG and DNA. Considering the growing interest in the application of electrospun nanofibers in the food industry, the ultra-efficient and safe antibacterial system was constructed using OG encapsulated with nanofibers by electrospinning and its synergetic sterilization effect was also ascertained on the microbial load of Chinese Taihu icefish (*Neosalanx taihuensis* Chen). This study is expected to provide a comprehensive view of the antimicrobial mechanism of OG on *E. coli* and *S. aureus*, and a novel case of food packaging applications via electrospinning technique combined with OG for food preservations.

2. Materials and methods

2.1. Materials

All experiments were performed in Luria-Bertani (LB) medium (Fisher Scientific). For bactericidal drug experiments in *E. coli* and *S. aureus*, gallic acid, methyl gallate and ethyl gallate (> 99%) were purchased from Aladdin (Shanghai, China). Silverfish (*Neosalanx taihuensis* Chen) was a gift from Prof. Beiwei Zhu in Dalian Polytechnic University and stored at -20 ^{o}C. All other chemicals of research or HPLC grade were purchased from commercial sources of China.

144 *2.2. Biocatalysis for preparation of alkyl gallates*

145 The biocatalysis was carried out according to our previously published paper (Shi et al., 2017; 2018)
146 with some modifications. More detailed procedures for preparing target compounds including
147 1-butanol (1-hexyl, 1-octyl, 1-decyl, 1-dodecyl and 1-tetradecyl) gallate were given in SI. The
148 structures of them were characterized by ^{1}H NMR and ^{13}C NMR.

149 *2.3. Bacterial strains and culture conditions*

150 *Escherichia coli* (*E. coli*) ATCC 25922 and *Staphylococcus aureus* (*S. aureus*) ATCC 6538 were
151 obtained from the National Center For Medical Culture Collections (Beijing, China). Cultures were
152 grown and maintained in LB broth and on LB agar (Hangzhou Microbial Reagent Co. Ltd, China).
153 Then, the pre-cultured bacterial cells were transferred to 20 mL LB broth in 150 mL flasks, and the
154 cells were cultivated to exponential phase at 37 ^{o}C at 180 rpm. They are used as indicator strains for
155 subsequent tests related to the inhibitory activity of GA and alkyl gallates.

156 *2.4. The uptake of GA and alkyl gallates in bacterial cells*

157 The uptake of GA and its esters was evaluated using diphenylboric acid 2-aminoethyl ester (DPBA),
158 a flavonoid specific dye according to the method of Wang et al. (2017). A volume of 1 mL of an
159 overnight culture of *E. coli* was transferred to a tube and centrifuged at 10000 g for 5 mins to obtain
160 a pellet (10^{9} CFU mL^{-1}). A volume of 1 mL of PBS (pH7.2, 0.1 M) containing GA and its esters (0.1
161 mM) was added to the pellet and mixed. After the incubation of 15, 30, 60 mins, each suspension
162 was transferred back to a tube and centrifuged at 10000 g for 5 mins. The supernatant was discarded
163 and the pellet was washed twice with PBS and then mixed with 450 μL of DPBA solution. The final
164 suspension of 100 μL was transferred to a 96-well plate and fluorescence intensity (λex/λem
165 =405/465 nm) was recorded by a hybrid multi-mode microplate reader (Synergy H1, Biotek). The
166 fluorescence intensity ratio was corrected using the following equation: Corrected fluorescence=
167 fluorescence intensity $_{\text{treated sample}}$ - fluorescence intensity $_{\text{control}}$. The uptake rates (μ) in *E. coli* and *S.*
168 *aureus* were calculated using values according to the following equation: $\mu = (\ln I_1 - \ln I_2)/(t_1 -$
169 $t_2) \times 100$, where I_1 and I_2 are the corrected fluorescence values at the culture times t_1 and time t_2,
170 respectively.

171 *2.5. Antimicrobial activity*

172 To determine the values of MIC and MBC, the assay was conducted according to our previously
173 published paper (Shi et al., 2019) with slight modifications. Both the growth curve assay and the

174 time-kill kinetics analysis were performed according to our previously published paper (Shi et al.,
175 2019). Detailed descriptions of these methods and analysis are given in SI.
176

177 *2.6. Alterations of the bacterial cell membrane*

178 *2.6.1. The damage of membrane permeability and integrity determination*

179 To evaluate the cell membrane integrity and permeability, membrane damage of *E. coli* and *S.*
180 *aureus* during the treatment was analyzed by using the fluorescence probe propidium iodide (PI),
181 the leakage of proteins and any 260 nm absorbing materials through membranes in *E. coli* and *S.*
182 *aureus* into supernatant and the electrical conductivity of the bacterial suspensions. They were
183 detected according to our previously published paper (Shi et al., 2018) with slight modifications.
184 Detailed descriptions of these methods and analysis are given in SI.

185 *2.6.2. Analysis of membrane fatty acids (MFAs)*

186 The extraction and transesterification of fatty acids were conducted using the method reported by
187 Zhu et al. (2014) with a little modification. 10 mL of bacterial cell sample and 25 mL Bligh-Dyer
188 extraction solution (deionized water: methanol: chloroform=4:10:5 (*v*/*v*/*v*) were added to a 50
189 mL-centrifuge tube and incubated at 4 ^{o}C overnight. Then, the mixture was centrifuged at 4000 g
190 for 10 mins at 4 ^{o}C and the supernatant was carefully removed. The remaining liquid is collected in
191 a test and then blown dry with nitrogen. The product was dissolved in 300 μL chloroform and added
192 to a separation column. The sample was eluted with 10 mL of chloroform, 10 mL of acetone, and 10
193 mL of anhydrous methanol. After adding anhydrous methanol, the sample was collected and dried
194 with nitrogen. 1 mL of a methanol toluene solution (*v*:*v*= 1:1) and 1 mL of 0.2 mol/L KOH
195 methanol solution were added to the test tube and placed in a 37 °C water bath for 15 mins. Add 0.3
196 mL of 1 mol/L acetic acid, 2 mL of n-hexane, 2 mL of deionized water, shake and separate, and
197 stratify at 1 h. The upper layer was carefully transferred to another tube and dried with nitrogen.
198 The hexane containing the internal standard nonadecaned acid methyl ester was added to the sample
199 vial through the organic phase filter membrane with a syringe, and the upper stage was tested. Fatty
200 acid methyl ester (FAME) analysis was performed with an Agilent Agilent GC 7890B coupled with
201 MS 5977B. And detailed descriptions of the method are given in SI.

202 *2.6.3. Scanning electron microscopy (SEM) observation*

203 SEM studies were conducted to confirm the efficacy of OG and the morphological alternations of

204 bacteria, according to our previously published paper (Shi et al., 2018) and detailed procedures
205 were given in SI.
206

207 *2.7. Interaction of OG with DNA*

208 The interaction of OG with DNA was investigated through UV-vis spectral data matrix and
209 chemometrics methods. Moreover, molecular docking experiments were performed to obtain further
210 information related to the binding mode and possible site between DNA and OG. And more detailed
211 descriptions of these experiments are given in SI. Agarose gel electrophoresis assay for the
212 detection of DNA-binding activity was performed based on the procedures described by Wang et al.
213 (2016). The pBR322 plasmid DNA (0.2 μg) in Tris–HCl/EDTA buffer (pH 7.2) was treated with the
214 different concentrations of OG, followed by dilution with the Tris–HCl buffer to a total volume of
215 20 μL. Then, the reaction mixtures were incubated at 37 ^{o}C for 1 h before being loaded onto a 1%
216 agarose gel, and the electrophoresis was performed for 35 mins under 110 V at room temperature.
217

218 *2.8. The generation of intracellular ROS*

219 *2.8.1. Intracellular ROS determination*

220 The bacterial cells were grown in LB at 37 ^{o}C to exponential phase and then diluted the final
221 concentration to 10^6 CFU mL^{-1}. The LB broth containing bacterial both suspension and OG with
222 the final concentrations of 0.1 mM was added to each flask to co-incubate for 2 h. The bacteria cells
223 were then harvested by centrifugation (6000 g, 4 ^{o}C) for 5 mins and resuspended with an equal
224 volume of PBS (pH=7.2, 0.1 M). To detect the overall ROS levels, 10 μL
225 2',7'-Dichlorodihydrofluorescein diacetate (DCFH-DA) with the final concentrations of 10 μM was
226 added to the above suspension. After co-incubation for 30 mins, the bacteria cells were washed
227 three times to remove extra fluorescence probe. The detection of fluorescence intensity at an
228 excitation wavelength of 484 nm and an emission wavelength of 525 nm.

229 *2.8.2. Intracellular hydroxyl radicals (•OH) determination*

230 As for further establishing intracellular •OH level in *E. coli*, the dye hydroxyphenyl fluorescein
231 (HPF), which is oxidized by •OH with high specificity (Setsukinai, Urano, Kakinuma, Majima, &
232 Nagano, 2003) was employed. Briefly, *E. coli* cells were incubated to exponential phase at 37 ^{o}C for
233 about 16 h and then diluted its final concentration to 10^6 CFU mL^{-1}. The LB broth containing

234 bacterial suspension and OG were added to each flask with the final concentrations of 0.1 mM and
235 incubated together for 2 h. To evaluate the intracellular •OH production in the exposed *E. coli*, 10
236 μM hydroxyphenyl fluorescein (HPF) was used as a specific fluorescein probe. The fluorescent
237 intensity (λex/λem =490/515 nm) was determined with the Synergy H1 Hybrid Microplate reader
238 (Biotek, USA) to detect •OH levels. For further visualization of intracellular •OH in both *E. coli*
239 and *S. aureus*, the fluorescent signal (λex/λem =490/515 nm) was recorded by CytoFLEX flow
240 cytometry (Beckman Coulter, USA).

241 *2.8.3. NAD^+/NADH level determination*

242 The Sigma-Aldrich analysis kit (MAK037) was used to evaluate the NAD^+/NADH ratio of bacterial
243 cells. The cells were washed with cold PBS (0.1 M, pH 7.2) and centrifuged at 2000 g for 5 mins.
244 Cells were extracted with 400 μL of NAD^+/NADH extraction buffer by homogenizing or
245 freezing/thawing for two cycles (20 mins) on dry ice followed by 10 mins at room temperature. To
246 remove insoluble, the sample was vortexed for 10 seconds and then centrifuged at 13000 g for 10
247 mins. The extracted NAD^+/NADH supernatant was transferred to labeled test tubes. The
248 supernatant was then used for NAD^+/NADH determination. Detailed descriptions of the method are
249 given in SI.

250 *2.8.4. ATP Determination.*

251 The bacterial was incubated in the LB broth to exponential phase at 37 ^oC for about 16 h and then
252 diluted its final concentration to 10^6 CFU mL^{-1}. Bacteria were treated with 0.1 mM OG,
253 respectively, add the same amount of solvent as the control group. At 0, 0.5, 1, 2 and 4 h, cells were
254 collected by centrifugation at 6000 g at 4 ^oC for 5 mins, washed three times with cold PBS (0.1 M,
255 pH 7.2), and then resuspended in 5 mL above PBS. The cell lysate was added and mix well, then
256 centrifuge at 12000 g at 4 ^oC for 20 mins. Collect the supernatant and store at low temperature. The
257 ATP level is detected by the ATP detection kit (Beyotime, Shanghai, China). Put the ATP detection
258 solution at room temperature for 3-5 mins, so that the ATP is completely consumed. Then, the
259 supernatant was mixed with 20 microliters of ATP detection solution, and its relative light unit
260 (RLU) was measured by using the Synergy H1 Hybrid Microplate reader (Biotek, USA).

261 *2.8.5. Malondialdehyde (MDA) and genome integrity determination*

262 The content of MDA in OG-exposed *E. coli* was quantified by the lipid peroxidation assay kit
263 (Beyotime, Shanghai, China) according to the manufacturer's instructions. Moreover, detailed

264 descriptions of the experiment regarding the genome integrity determination are shown in SI.

265 *2.8.6. Quantitative RT-PCR*

266 Total RNA was isolated using Bacteria Total RNA Isolation Kit (Sangon Biotech, Shanghai, China),
267 and cDNA was synthesized using a cDNA Synthesis SuperMix Kit (Hifair, Shanghai, China).
268 qRT-PCR was carried out using Hifair qPCR SYBR Green Master Mix kit (Hifair) and 16S rRNA
269 (Sangon). The expression of *ssrA* gene was used as an endogenous control to normalize the amount
270 of mRNA obtained from a target gene. Samples were run in triplicate. Detailed descriptions of the
271 method and the primers used are given in SI.
272

273 *2.9. Effects of a combination of OG with electrospun nanofiber on storage of Chinese icefish*

274 *2.9.1. Preparation of electrospinning solutions and nanofibers (NFs)*

275 The solutions for electrospinning and NFs were prepared using the method described by Liu et al.
276 (2018) with a slight modification. Detailed descriptions of the method are given in SI. The collected
277 nanofibers were used for the analysis of its morphology via scanning electron microscopy (SU8010,
278 Hitachi, Japan) (see Fig. S1) and the preservation of icefish (Fig. 5D).

279 *2.9.2. Storage test on Taihu icefish*

280 The preservation tests for Taihu icefish were performed to assess the preservation properties of
281 muti-functionalized nanofibers containing OG. Samples were treated through a 30 s immersion in
282 the *E. coli* suspension (10^3 CFU mL^{-1}) and then immediately dried and packaged in nanofibers mats.
283 All of the samples including control groups without the treatment of nanofibers were stored at 4 ^oC
284 for 15-30 days. The colony number was measured at intervals of 3 days, and each group was
285 measured three times in parallel. The bacteria were separated from the meat tissue surface by PBS
286 (0.1 M, pH 7.2) washing to collect the surviving bacteria. After serial dilution, samples were spread
287 on top of LB agar plates and incubated at 37 ^oC for 24 h for further counting of survivors. Finally,
288 the reduction rate of the bacteria population was calculated. To evaluate the quality of the icefish
289 with different treatments, the electronic nose was applied in the experiment (for more details was
290 given in SI and Fig. S2).
291
292

293 *2.10. Statistical analysis*

294 Each experiment was repeated three times and results were expressed as the mean ± standard
295 deviation (SD). Data were analyzed by ANOVA and Duncan's new multiple tests, which are
296 available in the Sigma Plot software (SPSS Inc., Chicago, IL, USA). $P<0.05$ were considered
297 significantly different.

298 **3. Results and discussion**

299 *3.1. Antibacterial activities of GA and its alkyl esters against model bacteria*

300 A series of alkyl esters were synthesized through the enzyme-mediated reactions (Shi et al., 2018)
301 and their MIC and MBC values against *E. coli* and *S. aureus* are shown in Table 1. Notably, it
302 appears that their inhibitory activities were correlated with the length of alkyl chains. More
303 specifically, MIC or MBC values first declined and then raised with the extension in the length of
304 the alkyl chain (Fig. 1A), which is known as the "cut-off effect". Moreover, gallate esters with
305 longer alkyl chain length exhibited a noticeable increase in the antibacterial activity, with 8-carbon
306 gallate against G– *E. coli* and 8-, 10-, 12-carbon gallate against G+ *S. aureus* resulting in the largest
307 increases in bactericidal activity. Also, lipophilicity, as an important parameter to expect the
308 biological activity of alkyl gallates, was also evaluated using the theoretical partition coefficients
309 (clog *P*) (Fig. S3). Since GA did show a relatively high MBC value against *E. coli* up to 6.4 mM,
310 the alkyl group must be mainly attributed to eliciting the antibacterial activity. In this case, the
311 growth of G– *E. coli* and G+ *S. aureus* were effectively inhibited by octyl gallate (OG), at very low
312 concentrations, presenting a MIC of 0.1 mM and MBC of 0.1 mM for *E. coli* and a MIC of 0.05
313 mM and MBC of 0.1 mM for *S. aureus*, respectively. Furthermore, the discrimination in values of
314 MIC and MBC of OG against both bacteria was not more than 2-fold, suggesting that its activity is
315 bactericidal. These data suggest that the antibacterial efficiency of alkyl gallates is close to the
316 extended length of the alkyl chain. Similar findings were reported by Kubo et al. (2002; 2004) for
317 alkyl gallates against G– *Salmonella choleraesuis* and G+ *Bacillus subtilis*. A parabolic relationship,
318 in fact, was found between the antibacterial activities of alkyl gallates and their lipophilicity and the
319 antibacterial activity was maximized at the alkyl chain length of C8 and C11 against *B. subtilis*,
320 while octyl(C8) gallate was the most effective against *S. choleraesuis*. Our recent findings also
321 showed that the antibacterial properties of alkyl ferulates against both *E. coli* and *L. monocytogenes*
322 were noted to be a parabolic function of the alkyl chain lengths and hexyl(C6) ferulate is found to
323 have the optimum alkyl chain length that maximizes the antibacterial performance (Shi et al., 2018;

2019). In addition, *S. aureus* was more susceptible to alkyl gallates than the G+ *E. coli*. The MIC and MBC values of OG against *S. aureus* are lower than those against *E. coli*, which is consistent with the results by Kubo et al. (2002; 2004). The envelope of G– and G+ bacteria greatly differ in their individual architecture, with that of the G– bacteria being the most complex one since it is composed of two distinct lipid membranes: an outer membrane (OM) and an inner membrane (IM) separated by a thin layer of peptidoglycan.

3.2. Cellular uptake

The length of the alkyl chain of these gallates is found to be associated with their biological actions (Kubo, Fujita, Nihei, & Nihei, 2004), such as antibacterial activity, but the precise role is still largely unknown. The cellular uptake of them in bacterial cells might provide a substantial basis for their antibacterial effects occurring in *vivo*. It is found that OG showed significantly the highest bio-uptake efficiency in *E. coli* and *S. aureus* samples for 30 and 60 mins compared to other gallates (Fig. S4). Moreover, the maximum uptaking rates (μ_{max}) of OG in *E. coli* and *S. aureus* was 58.0 min^{-1} and 67.6 min^{-1}, respectively, which was relatively higher than that of other gallates and GA (Fig. 1B). On the other hand, most of the tetradecyl(C14) gallate (TeG) was not uptaken into cells and remained in the water-based medium, probably in the form of an insoluble monolayer or spread film (Kubo, Xiao, Nihei, Fujita, Yamagiwa, & Kamikawa, 2002). Also, the uptake results of OG and TeG were consistent with the antibacterial results in Table 1. It is noteworthy that, however, although the antimicrobial activity of hexyl(C6) gallate (HG) was significantly higher than that of GA, bacteria treated with HG did not show a higher bio-uptake compared to GA, indicating that the inactivation toward the bacteria by HG followed a different mechanism than GA and the extent of bio-uptake may not be the only factor that affects their antibacterial effects. These data suggest that OG has a relatively higher affinity to the cell membrane than GA and other alkyl gallates. The mechanism of inactivation for OG is distinct from the corresponding GA, which is consistent with our previous findings related to t alkyl ferulates (Shi et al., 2018; 2019).

On the basis of the data obtained, the alkyl chain length greatly influences the antibacterial activities and the gallate with the optimized alkyl chain is able to enter into the membrane lipid bilayer portion to disorder the fluid bilayer of the membrane and even invade the cells. On the other hand, apart from the length of the alkyl chain, the data obtained so far suggest that biochemical mechanisms could play a more essential role in the antibacterial activity of alkyl gallates. Taken together, OG displayed drastically increased bacterial uptake, rendering outstanding antimicrobial effectiveness. Besides, it is currently permitted as an antioxidant additive in food (Sivasankaran,

357 Vikraman, Thomas, & Kumar, 2016). Therefore, these results prompted us to further investigate, in
358 more detail, the potential antibacterial mechanism of OG as a promising antimicrobial.
359
360 **[Table 1.]**
361 **[Fig. 1.]**
362

363 *3.3. Effect of OG on the bacterial growth and cellular membrane integrity*

364 Inhibitory activities of OG against *E. coli* and *S. aureus* were found to be dose- and time-dependent
365 (Fig. 1C). Interestingly, compared to G– *E. coli*, a significant decline of $OD_{600\,nm}$ of G+ *S. aureus*
366 with the exposure to OG at 1×MBC was maintained for 12 h, indicating the partial cell wall lysis
367 occurring induced by OG (Fig. 1C-b). However, this phenomenon can not be seen in Fig. 1C-a for *E.*
368 *coli*. The difference in lysis between *E. coli* and *S. aureus* may be due to the fact that G+ *S. aureus*
369 does not have an outer membrane preventing foreign molecule influx (Shi et al., 2019). The
370 antibacterial effect of OG was also evaluated by time-kill kinetics profiles against both bacterial
371 strains (Fig. 1D). OG treatment at the concentration higher than 0.1 mM generated a bactericidal
372 effect that reduced cell population to the limit of detection, demonstrating that *E. col*i and *S. aureus*
373 can be effectively exterminated by OG. Cells grown with OG showed a more severe phenotype and
374 decrease in size (Fig. 1E). On average, cell length decreased from 2.0 μm to 0.6 μm for *E. coli*,
375 from 0.8 μm to 0.5 μm for *S. aureus*, respectively.
376
377 PI can only enter into bacterial cells with damaged membranes and bind to nucleic acids, increasing
378 the fluorescence signals (Park & Kang, 2013). Therefore, PI uptake was used to characterize the
379 permeability of the (inner) membranes of *E. coli* and *S. aureus*. In Fig. 2A, the fluorescence
380 intensity of PI significantly increased in an OG concentration-dependent manner. Moreover, for *E.*
381 *coli* cells treated with OG at 1×MBC, PI uptake values maintain constant as the treatment time was
382 extended (Fig. 2A-a), whereas it significantly increased as the incubation time increased in *S.*
383 *aureus* exposed to 1×MBC OG (Fig. 2A-b). This may due to the lysis in *S. aureus* caused by OG
384 with relatively high concentrations, leading to more PI entering cytoplasm and binding to DNA.
385 This further corroborates the observed changes in Fig. 1C. Additionally, the values of samples from
386 both bacterial strains exposed to OG at 1×MBC sharply increased at 0.5 h. This result is consistent
387 with the data in Fig. 1D related to a rapid bactericidal property of OG at 1×MBC, clearly suggesting
388 that the antibacterial mechanism of OG was related to the cell membrane (Shi et al., 2018).
389

390 The leakage of cytoplasmic contents such as DNA, RNA and proteins, is an indicator of irreversible
391 damage in the bacterial cell membrane. Moreover, these nucleotides have strong UV absorptions at
392 260 nm. The leakage of 260 nm absorbing materials rapidly increased and then reached a plateau
393 afterward when *E. coli* and *S. aureus* cells were exposed to OG at 1×MBC (Fig. 2B).
394 Correspondingly, the leakage of proteins shows a similar pattern as the results in the release of
395 nucleotides (Fig. S5). We also measured the electrical conductivity of the bacterial suspensions and
396 found that samples in the treatment group exhibited higher conductivity (P<0.05) (Fig. S6). These
397 findings showed that OG could compromise the integrity of the membrane and lead to the
398 noticeable leakage of cytoplasmic contents from bacterial cytoplasm (Shi et al., 2018; Shen et al.,
399 2015). The difference in structural integrity between the control and treatment groups can be clearly
400 observed by using SEM analysis in Fig. 2C. Normal *E. coli* cells were rod-shaped with the smooth
401 surface (Fig. 2C-a), whereas the cell membrane of bacteria treated with OG was obviously ruined
402 with rough surfaces and tremendous membrane fragments (Fig. 2C-b). Moreover, the size of
403 OG-treated *E. coli* cells (<2.0 μm) became smaller compared with the control (~2.5 μm), indicating
404 that OG inhibits the growth of *E. coli*. Similarly, the cell deformation and morphological
405 alternations could be easily observed in *S. aureus* with the OG treatment (Fig. 2C-c,d). After 2 h,
406 cell adhesion and boundaries were unclear and the cell membranes were fractured. These findings
407 provided the indication that OG has very severe damage ability to bacterial morphology.
408
409 **[Fig. 2.]**
410

411 *3.4. Effect of OG on fatty-acids profiles in membranes of bacteria*

412 A total of 13 membrane fatty acids (MFAs) in *E. coli* and a total of 14 MFAs in *S. aureus* were
413 identified using GC−MS. Based on the GC−MS data, PCA analysis was utilized to discern which
414 MFAs were responsible for the difference between the control and samples exposed to OG. As
415 shown in Fig. S7, except for the control and ethanol groups, different groups formed distinct
416 clusters, inferring that the exposure of *E. coli* and *S. aureus* to OG may cause significant
417 discriminations in the MFAs composition for both bacterial strains. In Fig. 2D and Table S2, all 13
418 identified MFAs of G– *E.coli* were divided into three categories, saturated fatty acids (SFAs),
419 unsaturated fatty acids (UFAs) and cyclopropane fatty acids (CFAs). A significant increase in UFAs
420 (from 21.82% to 57.71%), coupled with a decrease of SFAs (from 78.18% to 42.29%) and CFAs
421 (from 9.73% to 4.87%), can be observed as *E. coli* cells were incubated with OG (from 0 to 0.05
422 mM) (Fig. 2D-a2). The increase in UFAs composition was mainly attributed to the increased

423 proportions of C18:2 and C18:1. On the other hand, the decrease in CFAs and SFAs was mainly due
424 to the declined proportions of C17:0*cyclo* and C19:0*cyclo*, C16:0 and C18:0, respectively. As shown
425 in Fig. S8, the ratios of SFAs to UFAs decreased with increasing concentrations of OG, which is
426 consistent with some previous reports showing that the proportion of UFAs and membrane fluidity
427 of *E. coli* would increase when they were exposed to naringenin (Wang et al., 2018). In addition, we
428 also found that the proportion of CFAs also reduced with the treatment of OG. According to the
429 previous report (Poger, & Mark, 2015), CFAs may not only stabilize membranes against adverse
430 environmental disturbances but also promote the cell membrane fluidity.
431
432 Correspondingly, a total of 14 MFAs of G+ bacteria, *S. aureus*, can be divided into unbranched
433 (UBFAs) and branched-chain fatty acids (BCFAs), wherein BCFAs include both *iso*- and
434 *anteiso*-BCFAs (Fig. 2D and Table S3). In Fig. 2D-b2 and S8, the relative proportion of UBFAs of *S.*
435 *aureus* incubated with OG at 1/3×MIC was increased to 70.52%, while *iso*- and *anteiso*-BCFAs
436 were reduced to 9.91% and 19.57%, respectively. The ratios of UBFAs to BCFAs were elevated
437 with an increase in OG concentrations, which was is inconsistent with some previous studies
438 demonstrating the increase in the proportion of BCFAs for some G+ bacteria exposed to the
439 antimicrobial stress (Wang et al., 2018; Sun et al.,2012). However, such alterations in MFAs were in
440 accordance with the other previous study showing that *S. aureus* responds to undesired conditions,
441 such as carvacrol and thymol or higher growth temperatures, by lowering the biosynthesis of iso
442 and *anteiso*C15:0 and increasing the levels of C16:0 and C18:0 (Di Pasqua, Hoskins, Betts, &
443 Mauriello, 2006).
444
445 Taken together, our data suggest that alterations in bacterial MFAs composition have the potential to
446 compromise cell wall structure and integrity, which render them sensitive to more than one
447 antimicrobial mechanism, resulting in a marked loss of bacterial survival.
448

449 *3.5. OG increased intracellular ROS generation and involvement of hydroxyl radicals*

450 Reactive oxygen species (ROS) are highly reactive chemical species. The main types of ROS
451 include free radicals, like superoxide anion radicals ($\bullet O_2^-$), hydrogen peroxide (H_2O_2), and the
452 highly reactive hydroxyl radicals (•OH). They are known to play a physiological role in
453 antimicrobial effect by reacting with biologically essential molecules such as lipids, proteins, and
454 nucleic acids, eventually resulting in the oxidative damage or even the death of organisms (Catala,
455 2012). Xiong et al. (2017) reported that the antibacterial activity of EGCG towards *E. coli* was

456 related to oxidative stress due to ROS generation, especially interior •OH radicals. As such, we
457 hypothesized that the ROS production induced by OG could be essential for OG-mediated killing.
458 Thus, the overall ROS generation was determined using an oxidation-sensitive fluorescent probe,
459 DCFH-DA. Fig. 3A shows that the ROS formation in bacterial cells was remarkably increased with
460 the concentration of OG. To further confirm which kind of ROS was mainly involved in
461 OG-mediated killing, the bacterial cells were incubated in the presence of commonly used
462 antioxidants (NAC and TEMPOL) and hydroxyl radicals (•OH) scavengers (DMSO and thiourea).
463 In Fig. 3B and 3C, exogenous TEMPOL did not reduce the antibacterial activity of OG, whereas
464 NAC significantly reduced the inhibitory activity. Furthermore, the presence of either DMSO or
465 thiourea significantly erased the inhibitory activity of OG. Thiourea as an effective •OH radicals
466 scavenger is known to mitigate the effects of •OH radicals in both eukaryotes and prokaryotes
467 (Touati et al., 1995). These results suggest that OG-induced intracellular •OH radicals might play a
468 vital role in OG-induced bacterial inhibition. Additionally, we incubated OG-exposed *E. coli* with
469 the iron chelator 2,2'-dipyridyl, which is an established means of blocking Fenton
470 reaction-mediated •OH radicals formation by sequestering unbound iron (Imlay, Chin & Linn,
471 1988). For the effect of 2,2'-dipyridyl and thiourea on the viability of bacteria grown in the
472 presence of OG as compared to the samples treated only with OG, a significant increase in bacterial
473 survival following the addition of 2,2'-dipyridyl and thiourea was observed (Fig. 3D), clearly
474 confirming that •OH radicals are involved in OG-induced cell death. These changes of •OH radicals
475 levels can be displayed in a more visible way using the flow cytometry with the dye hydroxyphenyl
476 fluorescein (HPF), which can be oxidized by •OH radicals with high specificity (Setsukinai, Urano,
477 Kakinuma, Majima, & Nagano, 2003). As depicted in Fig. 3E, the addition of OG led to an
478 increased level of intracellular •OH, whereas NAC, thiourea and 2,2'-dipyridyl noticeably reduced
479 the •OH levels in both bacterial cells exposed to OG, thus preventing both strains from the
480 subsequent adverse impacts of OG (Fig. 3D).
481
482 Furthermore, ROS-mediated lipid peroxidation, oxidation of proteins, and DNA damage are
483 well-known outcomes of ROS, leading to cellular damage and ultimately to cell death. MDA, a
484 product of lipid peroxidation, was quantitatively measured in *E. coli* treated with OG to evaluate the
485 potential lipid peroxidation. The contents of MDA increased significantly ($P<0.05$) by 1.13-fold in
486 the cell-free extracts of *E. coli* treated with 0.2 mM OG (Fig. S9), suggesting that •OH functioned
487 as an initiator of lipid peroxidation resulting in oxidative damage to the bacteria. Some reports
488 documented that lipid peroxidation of bacteria including *E. coli* caused by •OH generated via a
489 Fenton-like reaction (Catala, 2012; Hong, Kang, Michels, & Gadura, 2012). Besides, the genome

490 DNA image of agarose gel electrophoresis in Fig. 3F and S9 displayed that the bacterial genome
491 bands were more faint compare to the control, indicating that the damage of genomic integrity by
492 intracellular ROS induced by OG.
493
494 Inspired by these above observations in a link between OG's killing and ROS, we presumed that
495 OG should also affect the bacterial respiratory electron transport chain (ETC), which is a common
496 endogenous source of ROS. It is well known that the majority generation of superoxide could be
497 stimulated in bacterial cells through oxidation of the ETC driven by oxygen and the conversion of
498 NADH to NAD^+ (Kohanski, Dwyer, Hayete, & Lawrence, 2007). The increased superoxide ($\bullet O_2^-$)
499 production from ETC together with Fenton reaction fuels the formation of •OH radicals. In Fig. 3G,
500 NAD^+/NADH ratios are significantly increased by treatments with OG at 0.4 mM (1.98) compared
501 to the control (1.07), indicating the imbalance of the ETC. As high NAD^+/NADH signals disturbed
502 ETC activity, this should translate into energy production in the form of ATP, which can be regarded
503 as another indicator of ETC status (Lok et al., 2006). As expected, *E. coli* and *S. aureus* treated with
504 1×MIC of OG showed a rapidly enhanced ATP level during 2 h of treatment (Fig. S10). Considering
505 given the link between energetic perturbation and OG killing, the effect of these antioxidants (NAC
506 and TEMPOL) on intracellular ATP was next determined. In Fig. 3H and 3I, the addition of NAC
507 abrogated the OG induced ATP increase and NAC significantly improved *E. coli* survival after OG
508 exposure. In stark contrast, TEMPOL did not inhibit the OG-induced ATP increase. Accordingly, it
509 conferred no discernible protection against the OG-mediated killing. Taken together, these results
510 not only support the notion that ROS generation is related to the disturbance of ETC but also
511 cellular respiration and energetic perturbation are involved in OG lethality.
512
513 On the other hand, ROS may be generated by auto-oxidation or metal-catalyzed oxidation reactions.
514 OG is capable of inducing the production of superoxide anions ($\bullet O_2^-$) and H_2O_2 in the presence of
515 H-acceptor (Arkawa, Maeda, Okubo, & Shimamura, 2004). A possible mechanism of autoxidation
516 of OG (Akagawa et al., 2004; Chen et al., 2012) is also proposed in Fig. 5. After the formation of
517 $\bullet O_2^-$ and H_2O_2, the generation of •OH would be achieved by a Fenton reaction. Therefore, we
518 suggest that the pro-oxidant ability of OG plays an important role in ROS production.
519

520 *3.6. Expression analysis of ROS-related genes*

521 The expression of genes of SoxRS (*sodA*, *soxR* and *soxS*) and OxyR (*oxyR*, *ahpC*, *oxyS*, *dps*, *gor*,
522 *katG* and *ahpF* regulons) related to oxidative stress were investigated for the molecular basis of

523 redox stress responses. Results in Fig. 3J shows that with the OG treatment, the specific genes of
524 oxidative stress, *sodA*, *soxR* and *soxS*, were 3.47, 2.15 and 2.58 times, respectively, more expressed
525 than in the control. The hydrogen peroxide-inducible genes, *ahpC*, *oxyR*, *ahpF*, *oxyS* and *gorA* were
526 less expressed in treated cells with respect to control cells. It can be observed that
527 superoxide-related genes are up-regulated with the OG treatment, however, the genes that induce
528 hydrogen peroxide are down-regulated. These changes in the expression trend indicated that the
529 oxidative stress response was induced by OG.
530
531 **[Fig. 3.]**
532

533 *3.7. Effect of OG on DNA*

534 Since OG has the potential to reach the inner structure of cells through a damaged membrane, we
535 need to test whether OG may bind with DNA to inhibit gene expression, subsequently blocking the
536 enzyme and receptor synthesis, resulting in the death of bacteria. In Fig. 4A and S11, the spectrum
537 of DNA were characterized by a peak at 258 nm due to the absorption of purine and pyrimidine
538 bases of nucleic acids. To further confirm the interaction between OG and genomic DNA, spectral
539 data were combined into an expanded data matrix and resolved using the MCR-ALS method (Shi et
540 al., 2018). As shown in Fig. 4B, the extracted three pure spectra are assigned to free OG, free DNA,
541 and DNA–OG complexes by using the SVD model to the augmented data matrix. To further
542 confirm the binding mode and possible site between DNA and OG, molecular docking with 100
543 docking runs were conducted finally with the generation of 36 multimember conformational
544 clusters (Fig. S12). Ultimately, binding-position analysis for those two binding models (Fig.4C, D)
545 showed that OG inserted into the minor groove of DNA with the formation of H-bond between OG
546 and DNA. More specifically, OG was bound to A-T rich regions of DNA covered residues A5, A6,
547 A7, T7, T19, T20 both in site 1 and site 2 which can be attributed to A-T regions have narrower
548 space than G-C region and offer a better fit of small molecules into the minor groove like OG
549 (Ketan Sahoo et al., 2008). Agarose gel electrophoresis of free DNA and DNA exposed to OG was
550 employed to access whether it had DNA cleavage ability. These results imply that the interaction of
551 OG with DNA as the other antibacterial mechanisms may be involved as well.
552 **[Fig. 4.]**
553

554 *3.8. Proposed antibacterial mechanisms of OG against bacterial cells.*

555 Taken together, our results indicate that the action model of OG may be described as follows (Fig.
556 5A). First, OG can directly enter bacterial cells and inhibit the growth of bacterial cells. OG is able
557 to kill bacterial cells by causing membrane rupture and the leakage of cellular constituent materials.
558 Then, the internalized OG demolishes the bacterial cells through two pathways: (1) OG can
559 interfere with the activity of ETC on the cytoplasmic membrane, producing a high level of toxic
560 reactive species, which further contribute to cellular damage and death; and (2) interaction of OG
561 with DNA to disturb the gene replication of bacteria. It has been well accepted that the development
562 of antimicrobial resistance is not supposed to occur if the antimicrobial effect is attributed to
563 simultaneous interactions with multiple targets (Almeida, Faustino, & Tome, 2015).
564

565 *3.9. Nanofibers as active food packaging materials against icefish contamination*

566 Taihu Lake icefish is called "Taihu Sanbao" together with plum and white shrimp in China.
567 Foodborne pathogens, including *E. coli,* are easily introduced to icefish, leading to serious
568 economic losses and health threats. Therefore, effective methods to eliminate potential risks of
569 foodborne pathogens contamination in fish are crucial for the food industry and consumers. In this
570 scenario, PLA-based nanofibers incorporated with OG (Fig. S1), as a multifunctional food
571 packaging material, were delicately fabricated to extend the shelf life of icefish. In Fig. 5B, Without
572 PLA-based nanofiber wrapping, the survival of *E. coli* maintained a high level (10^8 CFU mL^{-1}) until
573 the end of the storage period at 4 ^oC. In sharp contrast, *E. coli* numbers in the fish with the
574 nanofiber treatment were found to decline to a lower level (10^3 CFU mL^{-1}) after 15 days of storage.
575 Besides, the electronic nose (Fig. S2) as a rapid technique is used to detect volatile compounds
576 related to quality changes during cool storage of fish products. In Fig. 5C and D, after 15 days
577 storage period, the data points of the fresh sample and samples wrapped with active nanofibers were
578 relatively close, demonstrating that the freshness of the processed fish does not change much. Our
579 research further confirmed that the PLA-based nanofibers with OG have unique superiorities for
580 maintaining the freshness of the icefish and prolonging its shelf life. Hence, such active packaging
581 materials are especially suitable for use in prolonging the shelf life of aquatic products.
582

583 **[Fig. 5.]**

584

585 **4. Conclusion**

586 In summary, this work studied the antibacterial properties of enzymatically synthesized alkyl
587 gallates. Their antibacterial activities are evidently related to not only the length of alkyl chains but
588 also the nature of microorganisms. Among them, OG exerted excellent antibacterial effectiveness
589 against *E. coli* and *S. aureus*. The antibacterial mechanism of OG was ascribed to the destruction of
590 the bacterial membrane and the toxic hydroxyl radical formation, as well as interacts with DNA.
591 OG was further incorporated into PLA to develop a novel functionalized nanofiber with outstanding
592 long-term antimicrobial and antioxidant activities, as an active food packaging material to
593 effectively extend the shelf life of Chinese Taihu icefish. Encouraged by these findings, we believe
594 that the combination of OG and the benefit of electrospun nanofibers can establish a highly efficient
595 multifunctional antibacterial system to address the growing challenges of foodborne infections in
596 the food industry.
597
598

599 **Acknowledgments**

600 The work was supported by National Natural Science Foundation of China (21106131), Zhejiang
601 Province Public Welfare Technology Application Research Project (LGJ19C200001), Academic
602 Exchanges and Talent Training Program (2017SICR109), Zhejiang Provincial Program for Overseas
603 High-Level Experts Introduction (Z20170407), as well as Food Science and Engineering the Most
604 Important Discipline of Zhejiang Province (JYTsp20142101).
605

606 **Abbreviation**

607 Gallic acid, GA
608 Methyl gallate, MG
609 Ethyl gallate, EG
610 Butanol gallate, BG
611 Hexyl gallate, HG
612 Octyl gallate, OG
613 Decyl gallate, DG
614 Dodecyl gallate, DoG

615 Tetradecyl gallate, TeG
616 Gallic acid esters, GAEs
617 Deep eutectic solvents, DES
618 Propidium iodide, PI
619 Diphenylboric acid 2-aminoethyl ester, DPBA
620 Reactive oxidative species, ROS
621 Hydroxyl radicals, •OH
622 Superoxide anion, $•O_2^-$
623 Electron transport chain, ETC
624 *Escherichia coli, E. coli*
625 *Staphylococcus aureus, S. aureus*

626 **References**

627 Akagawa, M., Shigemitsu, T., & Suyama, K. (2004). Production of hydrogen peroxide by
628 polyphenols and polyphenol-rich beverages under quasi-physiological conditions. *Bioscience*
629 *Biotechnology & Biochemistry, 67 (12),* 2632-2640.
630 Almeida, A., Faustino, M. AF, & Tome, J. PC (2015). Photodynamic inactivation of bacteria:
631 finding the effective targets. *Future Medicinal Chemistry, 7,* 1221-1224.
632 Arakawa, H., Maeda, M., Okubo, S., & Shimamura, T. (2004). Role of hydrogen peroxide in
633 bactericidal action of catechin. *Biological & Pharmaceutical Bulletin, 27 (3),* 277-281.
634 Borges, A., Ferreira, C., Saavedra, M. J., & Simões M. (2013). Antibacterial activity and mode of
635 action of ferulic and gallic acids against pathogenic bacteria. *Microbial Drug Resistance*, *19(4)*,
636 256-265.
637 Butt, M. S., & Sultan, M. T. (2009). Green tea: nature's defense against malignancies. *Critical*
638 *Reviews in Food Science Nutrition, 49 (5),* 463-473.
639 Catala, A. (2012). Lipid peroxidation. *In Principles of Free Radical Biomedicine, Chapter 7,*
640 137-159.
641 Chen, T., Liou, S., Wu, H., Tsai, F., Tsai, C., & Chang, Y. (2012). Amino acids with basic amino
642 side chain accelerate the pro-oxidant ability of polyphenolic compounds. *Food Chemistry, 134 (1),*
643 9-14.
644 Chirila, F., Tabaran, A., Fit, N., Nadas, G., Mihaiu, M., Tabaran, F., … Dan, S. D. (2017).
645 Concerning increase in antimicrobial resistance in Shiga toxin-producing *Escherichia coli* isolated
646 from young animals during 1980-2016. *Microbes & Environments, 32 (3),* 252-259.
647 Giftson, J. S., & Jayanthi, S. (2010). Chemopreventive efficacy of gallic acid, an antioxidant and

648 anticarcinogenic polyphenol, against 1, 2-dimethyl hydrazine induced rat colon carcinogenesis.
649 *Investigational New Drugs, 28 (3),* 251-259.
650 Hong, R., Kang, T. Y., Michels, C. A., & Gadura, N. (2012). Membrane lipid peroxidation in copper
651 alloy-mediated contact killing of *Escherichia coli*. *Applied & Environmental Microbiology, 78,*
652 1776-1784.
653 Imlay, J.A., Chin, S.M., & Linn, S. (1988). Toxic DNA damage by hydrogenperoxide through the
654 fenton reaction in vivo and in vitro. *Science, 240,* 640-642.
655 Kang, M. S., Oh, J. S., Kang, I. C., Hong, S. J., & Choi, C. H. (2008) Inhibitory effect of methyl
656 gallate and gallic acid on oral bacteria. *Journal of Microbiology, 46 (6),* 744-750.
657 Ketan Sahoo, B., Sundar Ghosh, K., Bera, R., & Dasgupta, S. (2008). Studies on the interaction of
658 diacetylcurcumin with calf thymus-DNA. *Chemical Physics, 351 (1-3),* 163-169.
659 Kim, S., Jun, C., Suk, K., Choi, B., Lim, H., Park, S., ... Shin, T. Y. (2006). Gallic acid inhibits
660 histamine release and pro-inflammatory cytokine production in mast cells. *Toxicological Sciences,*
661 *91 (1),* 123-131.
662 Kohanski, M. A., Dwyer, D. J., Hayete, B., & Lawrence, C. A. (2007). A common mechanism of
663 cellular death induced by bactericidal antibiotics. *Cell, 130 (5),* 797-810.
664 Kubo, I., Fujita, K., & Nihei, K. (2002). Anti-Salmonella activity of alkyl gallates. *Journal of*
665 *Agricultural & Food Chemistry, 50 (23),* 6692-6696.
666 Kubo I., Fujita, K., Nihei, K., & Masuoka, N. (2003). Non-antibiotic antibacterial activity of
667 dodecyl gallate. *Bioorganic & Medicinal Chemistry Letters, 11 (4),* 573-580.
668 Kubo, I., Fujita, K., Nihei, K., & Nihei, A. (2004). Antibacterial activity of alkyl gallates against
669 *bacillus subtilis*. *Journal of Agricultural & Food Chemistry, 52 (5),* 1072-1076.
670 Kubo, I., Xiao, P., Nihei, K., Fujita, K., Yamagiwa, Y., & Kamikawa, T. (2002). Molecular design of
671 antifungal agents. *Journal of Agricultural & Food Chemistry, 50 (14),* 3992-3998.
672 Li, T., Cui, F., Bai, F., Zhao, G., & Li, J. (2016). Involvement of acylated homoserine lactones
673 (AHLs) of aeromonas sobria in spoilage of refrigerated turbot (*Scophthalmus* maximus L.). *Sensors,*
674 *16 (7),* 1083.
675 Liu, Y., Liang, X., Wang, S., Qin, W., & Zhang, Q. (2018). Electrospun antimicrobial polylactic
676 acid/tea polyphenol nanofibers for food-packaging applications. *Polymers, 10 (5),* 561.
677 Lok, C., Ho, C., Chen, R., He, Q., Yu, W., Sun, H., ... Che, C. (2006). Proteomic analysis of the
678 mode of antibacterial action of silver. *Journal of Proteome Research, 5,* 916-924.
679 Lou, L., Osemwegie, O., & Ramkumar, S. S. (2012). Functional nanofibers and their applications.
680 *Industrial & Engineering Chemistry Research, 59(13)*, 5439–5455.
681 Luo, Q., Li, S., Liu, S., & Tan, H. (2017). Foodborne illness outbreaks in China, 2000-2014.

682 *International Journal of Clinical & Experimental Medicine, 10 (3),* 5821-5831.
683 Park, I. K., & Kang, D. H. (2013). Effect of electropermeabilization by ohmic heating for
684 inactivation of *Escherichia coli O157:H7*, *Salmonella enterica serovar typhimurium*, and *Listeria*
685 *monocytogenes* in buffered peptone water and apple juice. *Applied & Environmental Microbiology,*
686 *79 (23),* 7122-7129.
687 Poger, D., & Mark, A. E. (2015). A ring to rule them all: the effect of cyclopropane fatty acids on
688 the fluidity of lipid bilayers. *The Journal of Physics Chemical B, 119 (17),* 5487-5495.
689 Setsukinai, K., Urano, Y., Kakinuma, K., Majima, H.J., & Nagano, T. (2003). Development of novel
690 fluorescence probes that can reliably detect reactive oxygen species and distinguish specific species.
691 *The Journal of Biological Chemistry, 278,* 3170-3175.
692 Shen, S., Zhang, T., Yuan, Y., Lin, S., Xu, J., & Ye, H. (2015). Effects of cinnamaldehyde on
693 *Escherichia coli* and *Staphylococcus aureus* membrane. *Food Control, 47,* 196-202.
694 Shi, Y., Bian, L., Zhu, Y., Zhang, R., Shao, S., Wu, Y., … Sun, H. (2019). Multifunctional alkyl
695 ferulate esters as potential food additives: antibacterial activity and mode of action against *Listeria*
696 *monocytogenes* and its application on American sturgeon caviar preservation. *Food Control, 96,*
697 390-402.
698 Shi, Y., Wu, Y., Lu, X., Ren, Y., Wang, Q., Zhu, C., ... Wang, H. (2017). Lipase-catalyzed
699 esterification of ferulic acid with lauryl alcohol in ionic liquids and antibacterial properties in vitro
700 against three food-related bacteria. *Food Chemistry, 220,* 249-256.
701 Shi, Y., Zhu, Y., Shao, S., Zhang, R., Wu, Y., Zhu, C., ... Cai, W. (2018). Alkyl ferulate esters as
702 multifunctional food additives: antibacterial activity and mode of action against *Escherichia coli* in
703 vitro. *Food Chemistry, 66 (45),* 12088-12101.
704 Sivasankaran, U., Vikraman, A. E., Thomas, D., & Kumar, K. G. (2016). Nanomolar level
705 determination of octyl gallate in fats and oils. *Food Analytical Methods, 9 (7),* 2115-2123.
706 Sun, Y., Wilkinson, B. J., Standiford, T. J., Akinbi, H. T., & Riordan, M. X. D. O. (2012). Fatty
707 acids regulate stress resistance and virulence factor production for *Listeria monocytogenes*. *Journal*
708 *of Bacteriology, 194*, 5274-5284.
709 Touati, L. E., Jacques, M., Tardat, B., Bouchard, L., Despied, S., Monod, I. J., ... Recherche, D.
710 (1995). Lethal oxidative damage and mutagenesis are generated byiron in delta fur mutants of
711 *Escherichia coli*: protective role of superoxide dismutase. *Journal of Bacteriology, 177,* 2305-2314.
712 Wang, L., Wang, M., Zeng, X., Zhang, Z., Gong, D., & Huang, Y. (2016). Membrane destruction
713 and DNA binding of *Staphylococcus aureus* cells induced by carvacrol and its combined effect with
714 a pulsed electric field. *Journal of Agricultural & Food Chemistry, 64,* 6355-6363.
715 Wang, L., Zeng, X., Wang, M., Brennan, C. S., & Gong, D. (2018). Modification of membrane

716 properties and fatty acids biosynthesis-related genes in *Escherichia coli* and *Staphylococcus aureus*:
717 Implications for the antibacterial mechanism of naringenin. *Biochimica Et Biophysica Acta*
718 *Biomembranes, 1860 (2),* 481-490
719 Wang, Q., De Oliveira, E. F., Alborzi, S., Bastarrachea, L. J., & Tikekar, R. V. (2017). On
720 mechanism behind UV-A light enhanced antibacterial activity of gallic acid and propyl gallate
721 against *Escherichia coli* O157:H7. *Scientific Reports, 7,* 1-11.
722 Wu, Y., Shi, Y., Zheng, X., Dang, Y., Zhu, C., Zhang, R., ... Li, J. (2020). Lipophilic ferulic acid
723 derivatives protect PC12 cells against oxidative damage: Via modulating β-amyloid aggregation and
724 activating Nrf2 enzymes. *Food & Function, 11,* 4707-4718.
725 Xiong, L., Chen, Y., Tong, J., Huang, J., Li, J., & Gong, Y. (2017). Tea polyphenol epigallocatechin
726 gallate inhibits *Escherichia coli* by increasing endogenous oxidative stress. *Food Chemistry, 217,*
727 196-204.
728 Zhu, B., Xia, X., Xia, N., Zhang, S., & Guo, X. (2014). Modification of fatty acids in membranes of
729 bacteria: implication for an adaptive mechanism to the toxicity of carbon nanotubes. *Environmental*
730 *Science & Technology, 48 (7),* 4086-4095.
731

732 **TABLES and FIGURE Legends**

733 **Table 1.** MIC and MBC of **GA** and its alkyl ester derivatives against *E. coli* and *S. aureus*.

734

735 **Fig. 1.** (**A**) Correlation between the antimicrobial activity of GA and alkyl gallates against *E. coli*
736 and *S. aureus* and the number of carbon atoms in the alkyl chain. The best curve fit was obtained
737 with the polynomial equation $y=-0.0328x^2+0.50617x+1.85765$ by *E. coli* and
738 $y=-0.0259x^2+0.50826x+1.6352$ by *S. aureus.* (**B**) Maximum uptaking rate (μ_{max}) of GA and its alkyl
739 gallates in *E. coli* and *S. aureus*. Data represent the mean value ± SD (n=3). Different letters means
740 significant differences ($P < 0.05$). (**C**) The growing curves indicate a growth inhibition of OG
741 against *E. coli* and *S. aureus*. (**D**) Time-kill kinetics profiles of OG against *E. coli* and *S. aureus*.
742 The cell number was determined after plating serial dilutions and counting the CFU. Each value is
743 the mean ± SD of three replicates. (**E**) Cell length distribution of cells grown of *E. coli* and *S.*
744 *aureus* without or with 1×MIC OG for 2 h.

745

746 **Fig. 2**. (**A**) Uptake of PI in (**a**) *E. coli* and (**b**) *S. aureus.* (**B**) The leakage of both UV-absorbing
747 substances ($OD_{260\ nm}$) and proteins of bacteria treated without or with OG (1×MIC and 1×MBC) for
748 0.5 h, 1 h, 2 h and 4 h. (**C**) Scanning electron microscopy (SEM) of (**a**) *E. coli* and (**c**) *S. aureus*
749 without OG treatment, (**b**) and (**d**) with OG treatment at 1×MBC for 2 h. (**D**) The relative
750 proportions of different MFAs species in (**a1**) *E. coli* and (**b1**) *S. aureus*. Total SFAs and UFAs
751 proportions in the cytoplasmic membrane of (**a2**) *E. coli* and total BCFAs and UBFAs proportions
752 in the cytoplasmic membrane of (**b2**) *S. aureus* when grown with different concentrations of OG.
753 Data represent the mean value ± SD (n=3). The superscript (*) indicates significantly different to
754 equivalent control points ($P<0.05$)

755

756 **Fig. 3**. (**A**) The generation of ROS in *E. coli* and *S. aureus* treated with OG by using the dye
757 2',7'-Dichlorodihydrofluorescein diacetate (DCFH-DA). *$P < 0.05$ (vs the control group). (**B**) Effect
758 of antioxidants including NAC or TEMPOL on the growth of *E. coli* in LB with 0.1 mM OG. (**C**)
759 Effect of hydroxyl radical scavengers including DMSO (0.7 M) or Throurea (150 mM) on the
760 growth of *E. coli* treated with OG. (**D**) The viability of *E. coli* was determined after exposure to 0.1
761 mM OG (with 0.7 M DMSO or 150 mM thiourea) for 6 h. (**E**) Generation of hydroxyl radicals in *E.*
762 *coli* and *S. aureus* following exposure to 0.1 mM OG in the absence or presence of 100 μM
763 2,2'-dipyridyl or 150 mM thiourea or 4 mM NAC. (**F**) Fragmented DNA in OG-treated *E. coli*. (**G**)
764 Fold change in NAD^+/NADH (nmol/mL) following the treatment with OG. (**H**) ATP concentration
765 in *E.coli* treated with OG in the absence or presence of 4 mM NAC or 4 mM TEMPOL for 4 h prior

766 to ATP measurement. (**I**) The viability of *E. coli* was determined after exposure to 0.1 mM OG (with
767 4 mM NAC or 4 mM TEMPOL) for 24 h. *P < 0.05; **P < 0.01; ***P < 0.001 (vs the group
768 treated with 0.1 mM OG alone). (**J**) Relative expression of selected genes controlled by SoxRS and
769 OxyR regulons during *E. coli* growth in the presence or absence of the OG for 12 h. Error bars
770 represent ±SD of the mean. *P < 0.05; **P < 0.01; ***P < 0.001 relative to the control.
771
772 **Fig. 4.** (**A**) UV-vis spectra obtained from OG with increasing concentration of genomic DNA
773 (**Experiment 1**), The initial concentration of OG was 5×10^{-5} M, while the concentration of DNA
774 was 0, 0.29, 0.58, 0.87,..., 7.25×10^{-5} M for curves 1 to 26; (**B**) Recovered results by MCR-ALS.
775 Molecular modeling posture of the DNA−OG system at (**C**) site 1 and (**D**) site 2. The area marked
776 in green is hydrogen bonds.
777
778 **Fig. 5**. Schematic mechanisms for the antibacterial activity of OG. (1) OG damages the membrane
779 of bacterial cells and easily permeates into the intact cells and then (2) interacts with DNA to
780 disturb the gene replication of bacteria. (3) OG disrupts the activity of ETC on the cytoplasmic
781 membrane to generate a high level of toxic ROS. The changes in preservation quality indices of
782 *Neosalanx taihuensis* Chen during storage at 4 ^{o}C. (**B**) Numbers of *E. coli* surviving on the
783 *Neosalanx taihuensis* Chen during storage at 4 ^{o}C. (**C**) PCA analysis of volatile odors of *Neosalanx*
784 *taihuensis* Chen. (**a**) fresh fish before the storage; Treatment with nanofiber for 6 days (**b**) and 15
785 days (**c**); Treatment without nanofiber for 6 days (**d**) and 15 days (**e**). (**D**) The appearance of the
786 packed *Neosalanx taihuensis* Chen in the absence and presence of electrospun nanofibers (CNFs)
787 containing OG during 15 days of storage at 4 ^{o}C.
788
789

790

791 **Table 1**

792

793 **Table 1.** MIC and MBC of **GA** and its alkyl ester derivatives against *E. coli* and *S. aureus*.

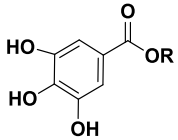		R	*E. coli* (G^-)		*S. aureus* (G^+)		$c\log P^a$
			MIC (mM)	MBC (mM)	MIC (mM)	MBC (mM)	
Gallic acid	Gallic acid (**GA**)	H	3.2	6.4	3.2	>6.4	0.4254
Gallate	Methyl Gallate (**MG**)	C_2H_5	3.2	>6.4	3.2	>6.4	1.4603
	Butyl Gallate (**BG**)	C_4H_9	3.2	3.2	3.2	3.2	2.9173
	Hexyl Gallate (**HG**)	C_6H_{13}	0.2	0.8	0.2	0.8	3.5764
	Octyl Gallate (**OG**)	C_8H_{17}	0.1	0.2	0.05	0.1	4.6344
	Decyl Gallate (**DG**)	$C_{10}H_{21}$	0.8	6.4	0.05	0.05	5.6924
	Dodecyl Gallate (**DoG**)	$C_{12}H_{25}$	0.8	6.4	0.05	0.05	6.7503
	Tetradecyl Gallate (**TeG**)	$C_{14}H_{29}$	3.2	6.4	1.6	1.6	7.8084

794 [a] Theoretical estimated using ChemBioDraw Ultra 13.0 program.

795

796

797 **Figure captions**

798 *Shi et al.*

799

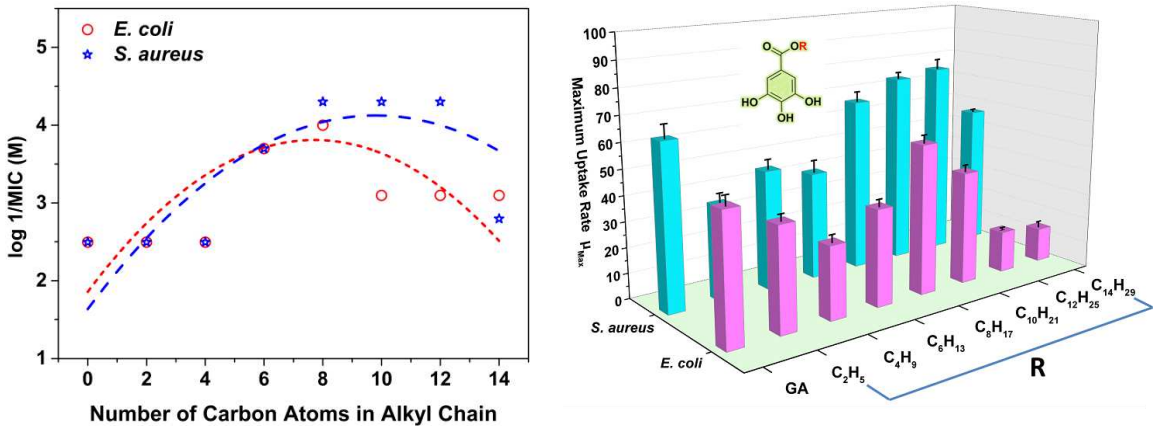

(A) **(B)**

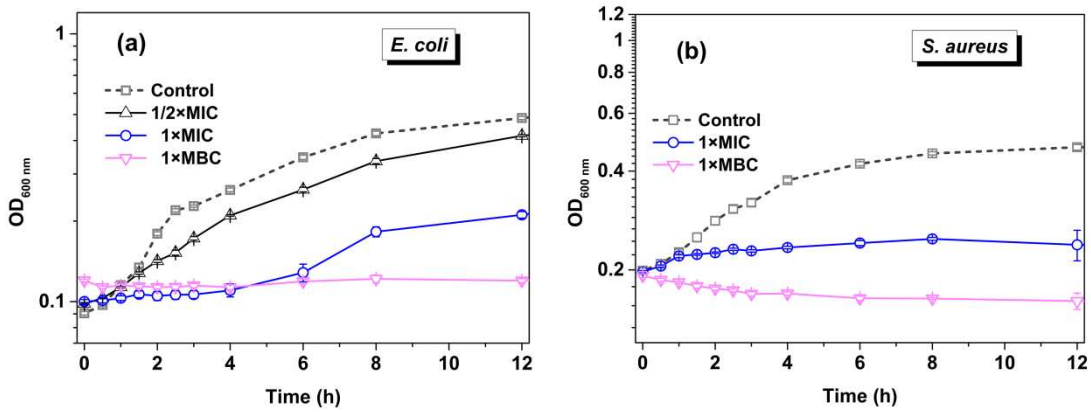

(C)

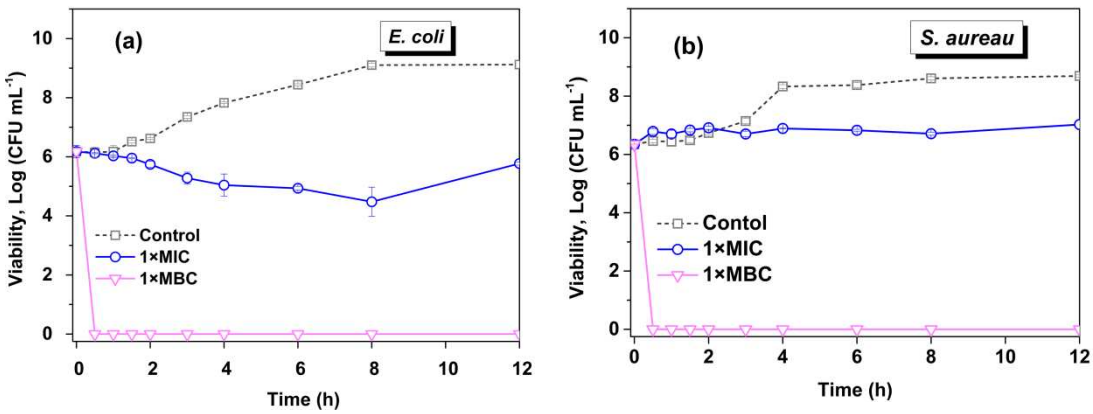

(D)

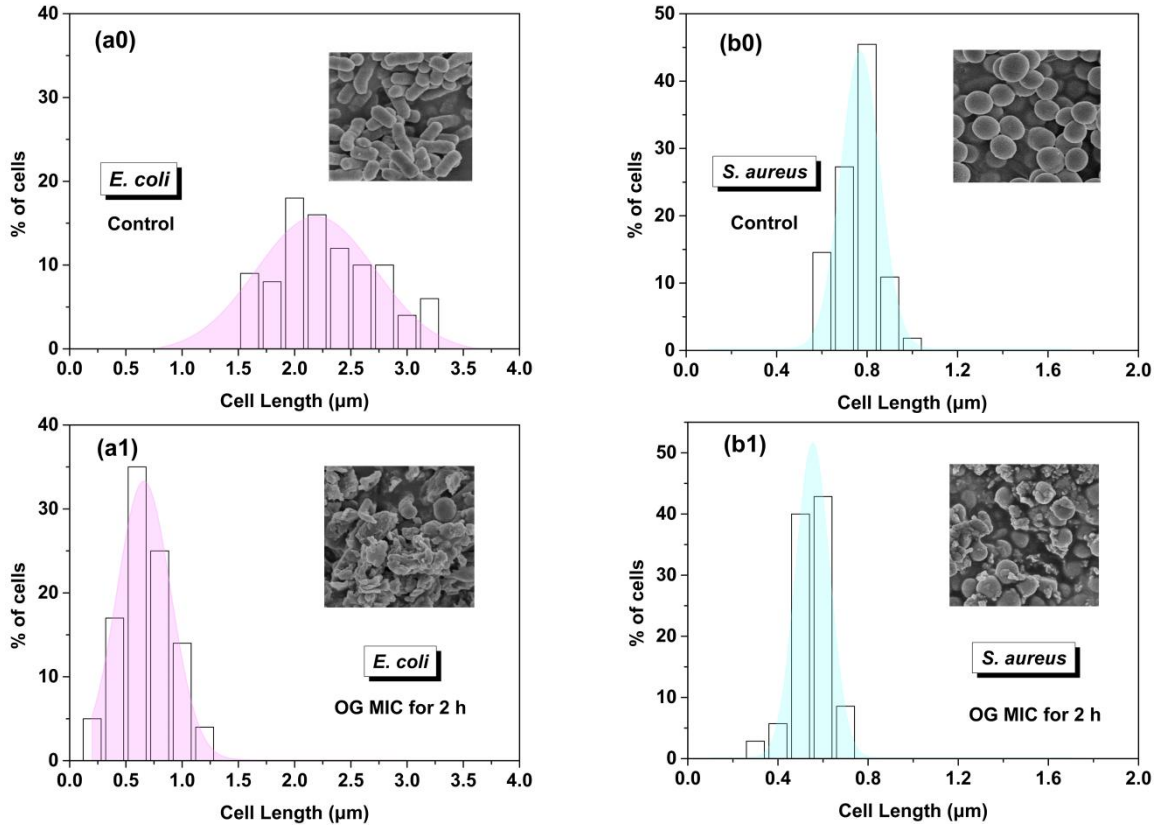

(E)

Fig. 1. (**A**) Correlation between the antimicrobial activity of GA and alkyl gallates against *E. coli* and *S. aureus* and the number of carbon atoms in the alkyl chain. The best curve fit was obtained with the polynomial equation y= $-0.0328x^2+0.50617x+1.85765$ by *E. coli* and y= $-0.0259x^2+0.50826x+1.6352$ by *S. aureus.* (**B**) Maximum uptaking rate (μ_{max}) of GA and its alkyl gallates in *E. coli* and *S. aureus*. Data represent the mean value ± SD (n=3). Different letters means significant differences ($P < 0.05$). (**C**) The growing curves indicate a growth inhibition of OG against *E. coli* and *S. aureus*. (**D**) Time-kill kinetics profiles of OG against *E. coli* and *S. aureus*. The cell number was determined after plating serial dilutions and counting the CFU. Each value is the mean ± SD of three replicates. (**E**) Cell length distribution of cells grown of *E. coli* and *S. aureus* without or with 1×MIC OG for 2 h.

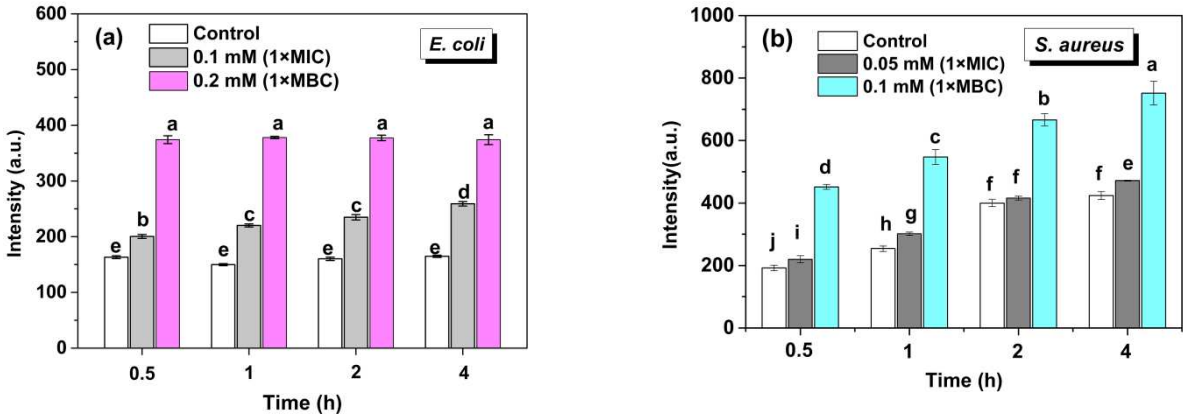
(a)
Control
0.1 mM (1×MIC)
0.2 mM (1×MBC)
E. coli
Intensity (a.u.)
Time (h)
(b)
Control
0.05 mM (1×MIC)
0.1 mM (1×MBC)
S. aureus
Intensity(a.u.)
Time (h)

(**A**)

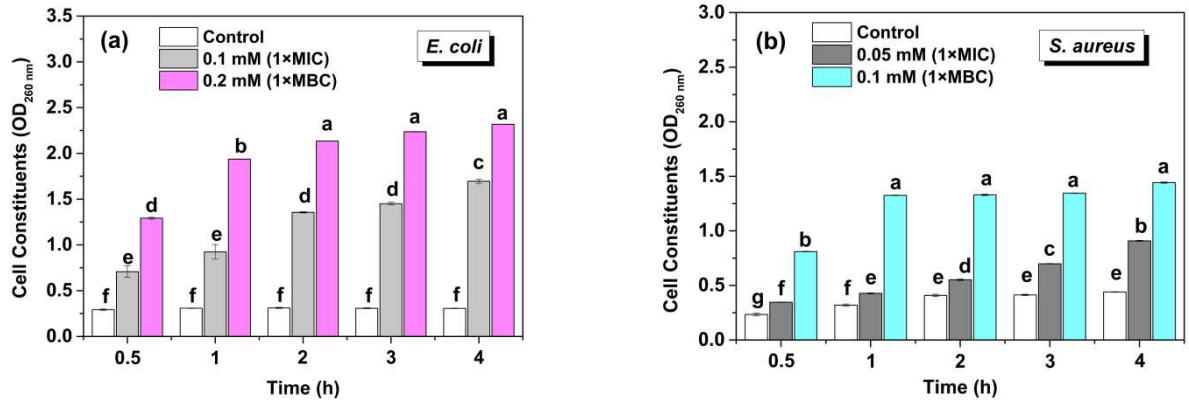
(a)
Control
0.1 mM (1×MIC)
0.2 mM (1×MBC)
E. coli
Cell Constituents (OD260 nm)
Time (h)
(b)
Control
0.05 mM (1×MIC)
0.1 mM (1×MBC)
S. aureus
Cell Constituents (OD260 nm)
Time (h)

(**B**)

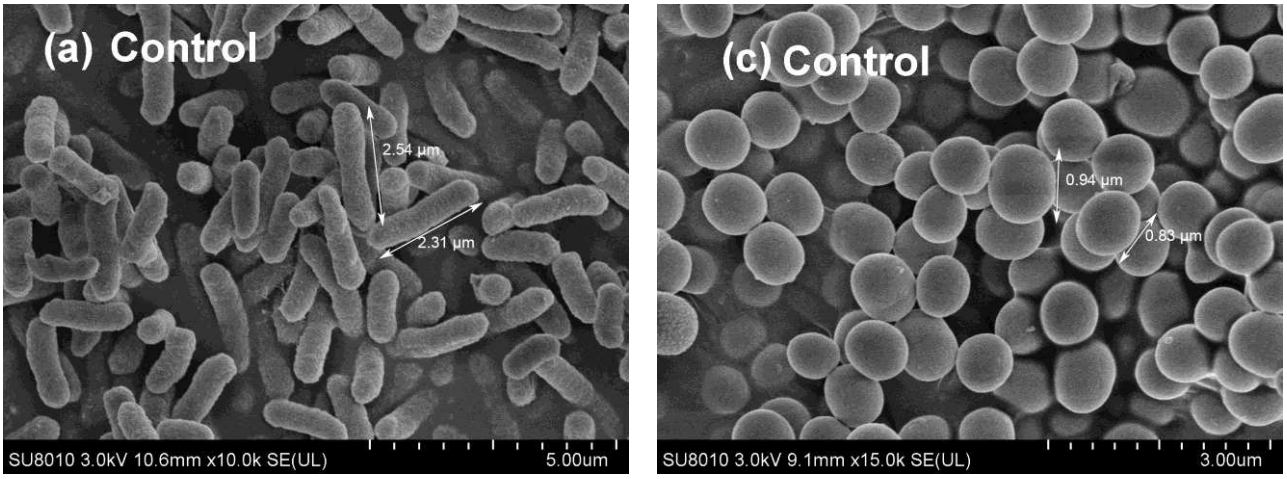
(a) Control
2.54 μm
2.31 μm
SU8010 3.0kV 10.6mm x10.0k SE(UL)
5.00um
(c) Control
0.94 μm
0.83 μm
SU8010 3.0kV 9.1mm x15.0k SE(UL)
3.00um

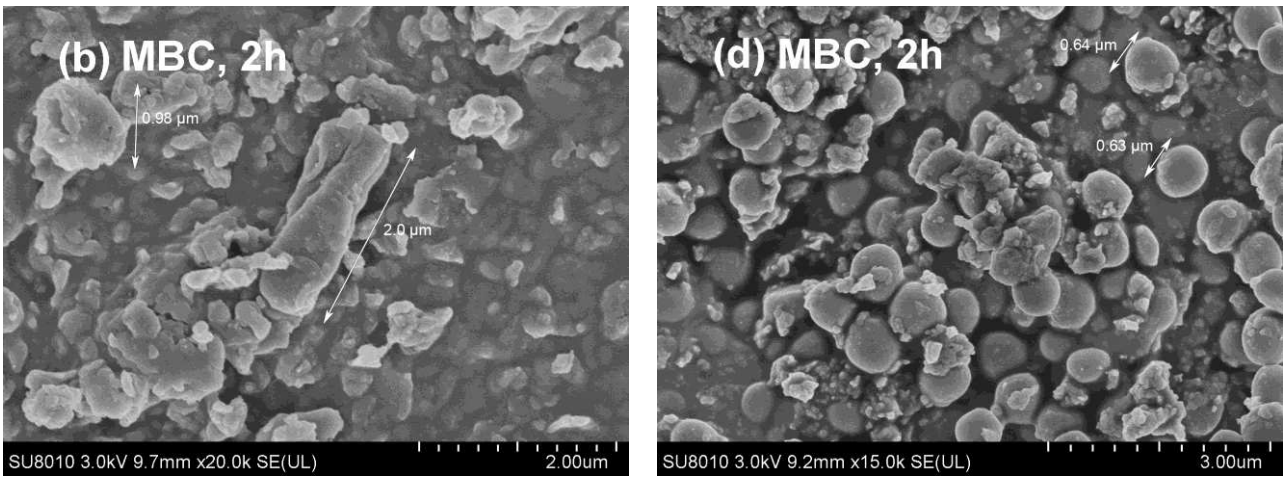

(C)

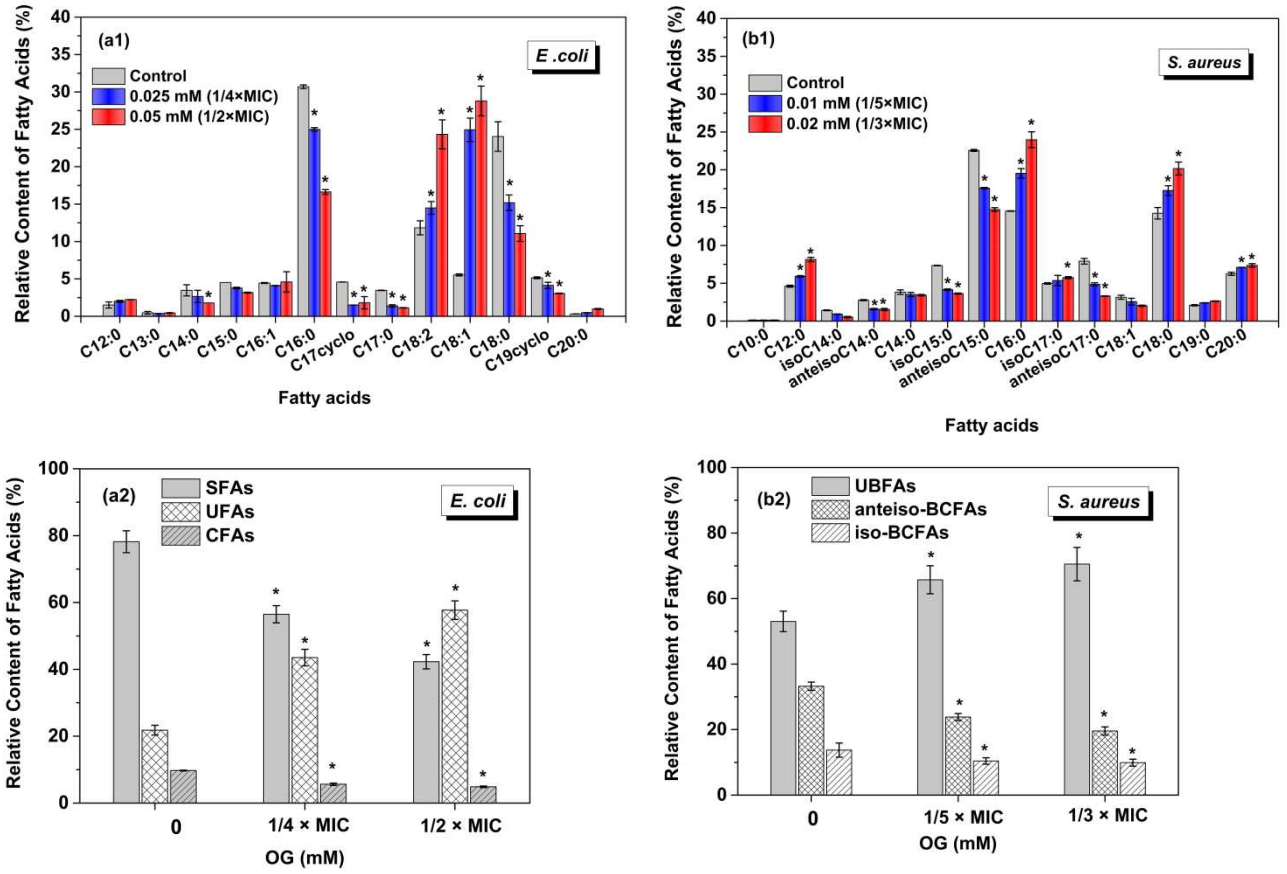

(D)

Fig. 2. (**A**) Uptake of PI in (**a**) *E. coli* and (**b**) *S. aureus.* (**B**) The leakage of both UV-absorbing substances ($OD_{260\ nm}$) and proteins of bacteria treated without or with OG (1×MIC and 1×MBC) for 0.5 h, 1 h, 2 h and 4 h. (**C**) Scanning electron microscopy (SEM) of (**a**) *E. coli* and (**c**) *S. aureus* without OG treatment, (**b**) and (**d**) with OG treatment at 1×MBC for 2 h. (**D**) The relative proportions of different MFAs species in (**a1**) *E. coli* and (**b1**) *S. aureus*. Total SFAs and UFAs proportions in the cytoplasmic membrane of (**a2**) *E. coli* and total BCFAs and UBFAs proportions

822 in the cytoplasmic membrane of (**b2**) *S. aureus* when grown with different concentrations of OG.
823 Data represent the mean value ± SD (n=3). The superscript (*) indicates significantly different to
824 equivalent control points ($P<0.05$)
825
826
827
828

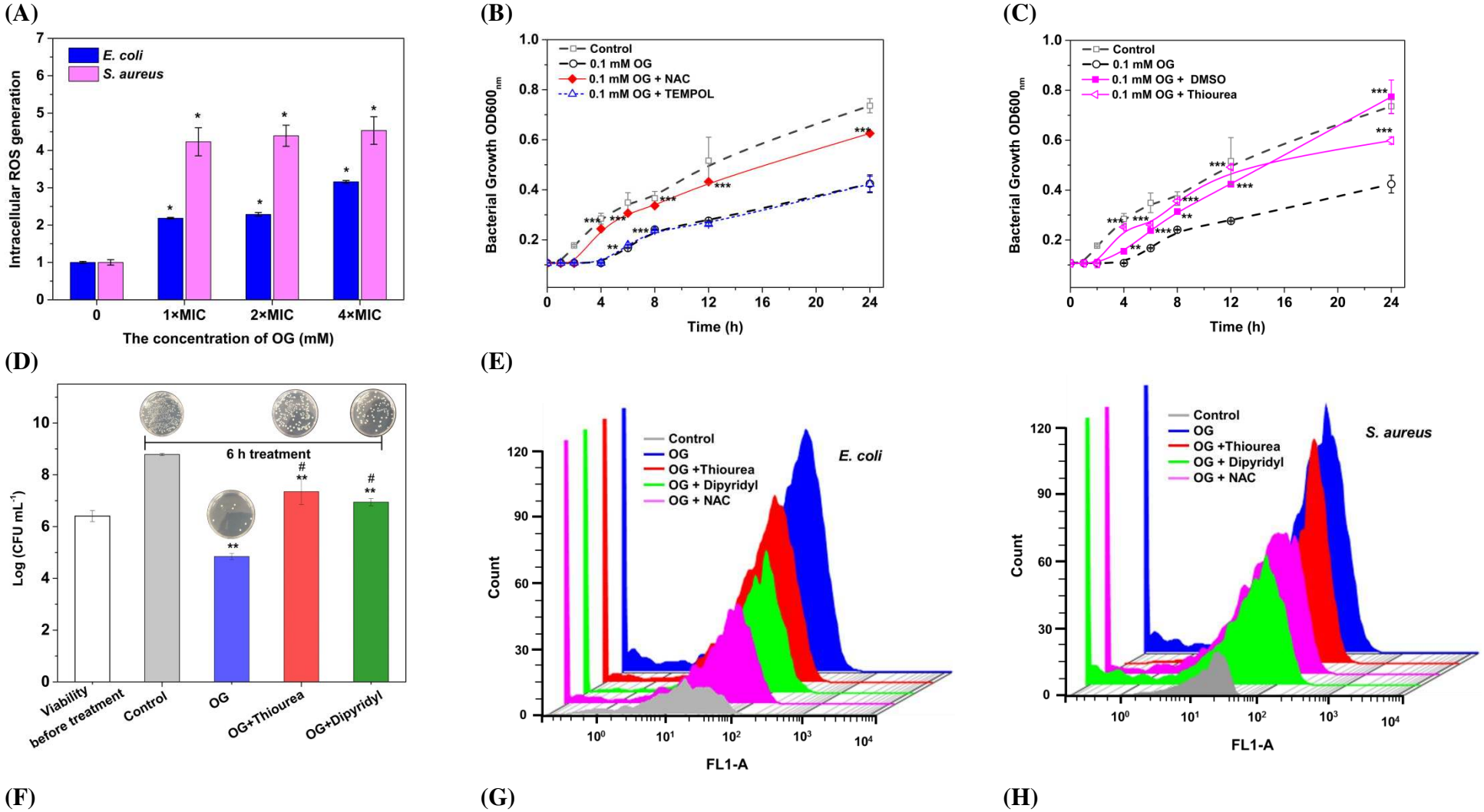
(A)
E. coli
S. aureus
Intracellular ROS generation
0
1×MIC
2×MIC
4×MIC
The concentration of OG (mM)
(B)
Control
0.1 mM OG
0.1 mM OG + NAC
0.1 mM OG + TEMPOL
Bacterial Growth OD600nm
Time (h)
(C)
Control
0.1 mM OG
0.1 mM OG + DMSO
0.1 mM OG + Thiourea
Bacterial Growth OD600nm
Time (h)
(D)
6 h treatment
Log (CFU mL-1)
Viability before treatment
Control
OG
OG+Thiourea
OG+Dipyridyl
(E)
Control
OG
OG +Thiourea
OG + Dipyridyl
OG + NAC
E. coli
Count
FL1-A
(G)
Control
OG
OG +Thiourea
OG + Dipyridyl
OG + NAC
S. aureus
Count
FL1-A
(F)
(H)

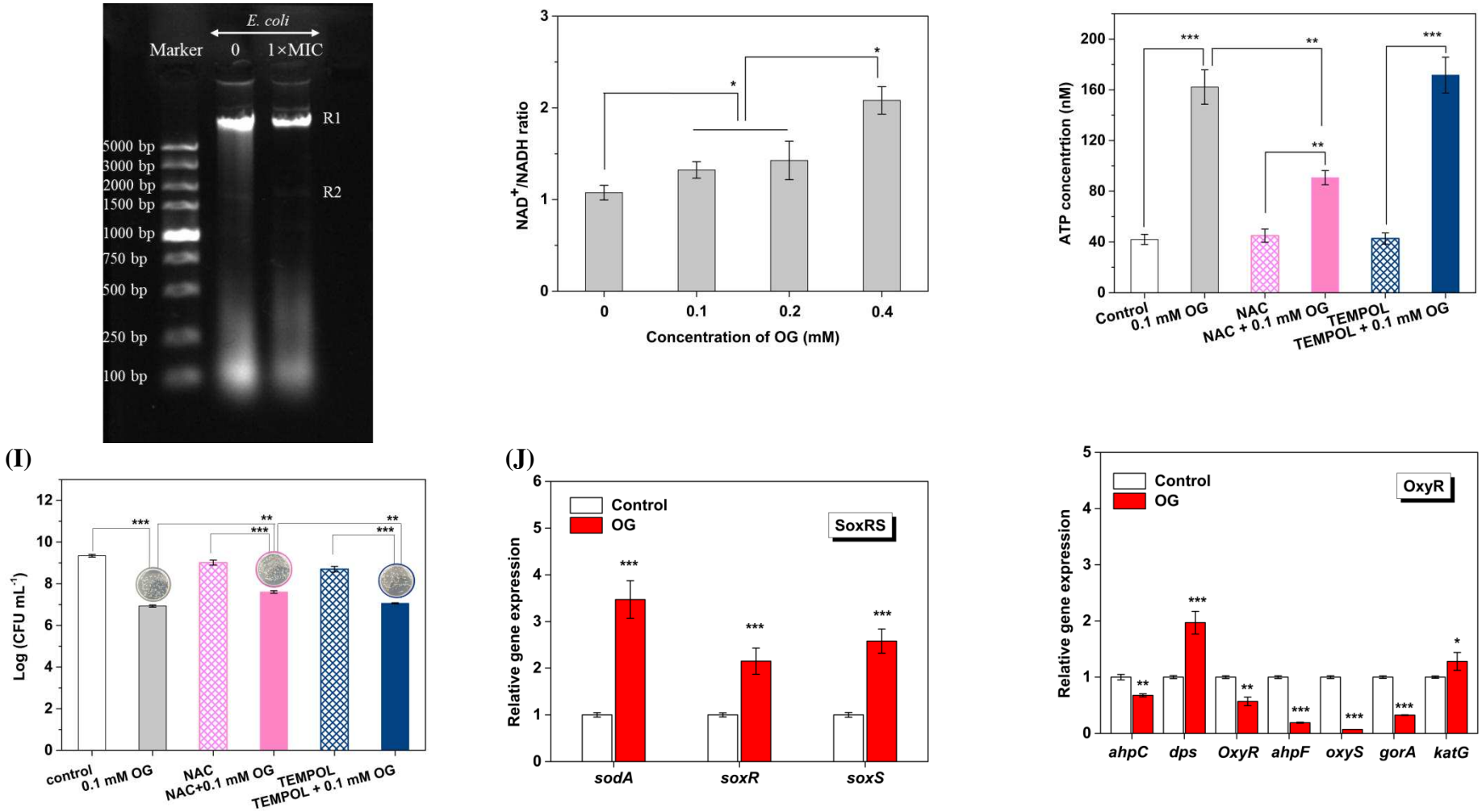

Fig. 3. (**A**) The generation of ROS in *E. coli* and *S. aureus* treated with OG by using the dye 2',7'-Dichlorodihydrofluorescein diacetate (DCFH-DA). *$P < 0.05$ (vs the control group). (**B**) Effect of antioxidants including NAC or TEMPOL on the growth of *E. coli* in LB with 0.1 mM OG. (**C**) Effect of hydroxyl radical scavengers including DMSO (0.7 M) or Throurea (150 mM) on the growth of *E. coli* treated with OG. (**D**) The viability of *E. coli* was

834 determined after exposure to 0.1 mM OG (with 0.7 M DMSO or 150 mM thiourea) for 6 h. (**E**) Generation of hydroxyl radicals in *E. coli* and *S. aureus*
835 following exposure to 0.1 mM OG in the absence or presence of 100 μM 2,2'-dipyridyl or 150 mM thiourea or 4 mM NAC. (**F**) Fragmented DNA in
836 OG-treated *E. coli*. (**G**) Fold change in NAD^+/NADH (nmol/mL) following the treatment with OG. (**H**) ATP concentration in *E.coli* treated with OG in
837 the absence or presence of 4 mM NAC or 4 mM TEMPOL for 4 h prior to ATP measurement. (**I**) The viability of *E. coli* was determined after exposure
838 to 0.1 mM OG (with 4 mM NAC or 4 mM TEMPOL) for 24 h. *$P < 0.05$; **$P < 0.01$; ***$P < 0.001$ (vs the group treated with 0.1 mM OG alone). (**J**)
839 Relative expression of selected genes controlled by SoxRS and OxyR regulons during *E. coli* growth in the presence or absence of the OG for 12 h.
840 Error bars represent ±SD of the mean. *$P < 0.05$; **$P < 0.01$; ***$P < 0.001$ relative to the control.

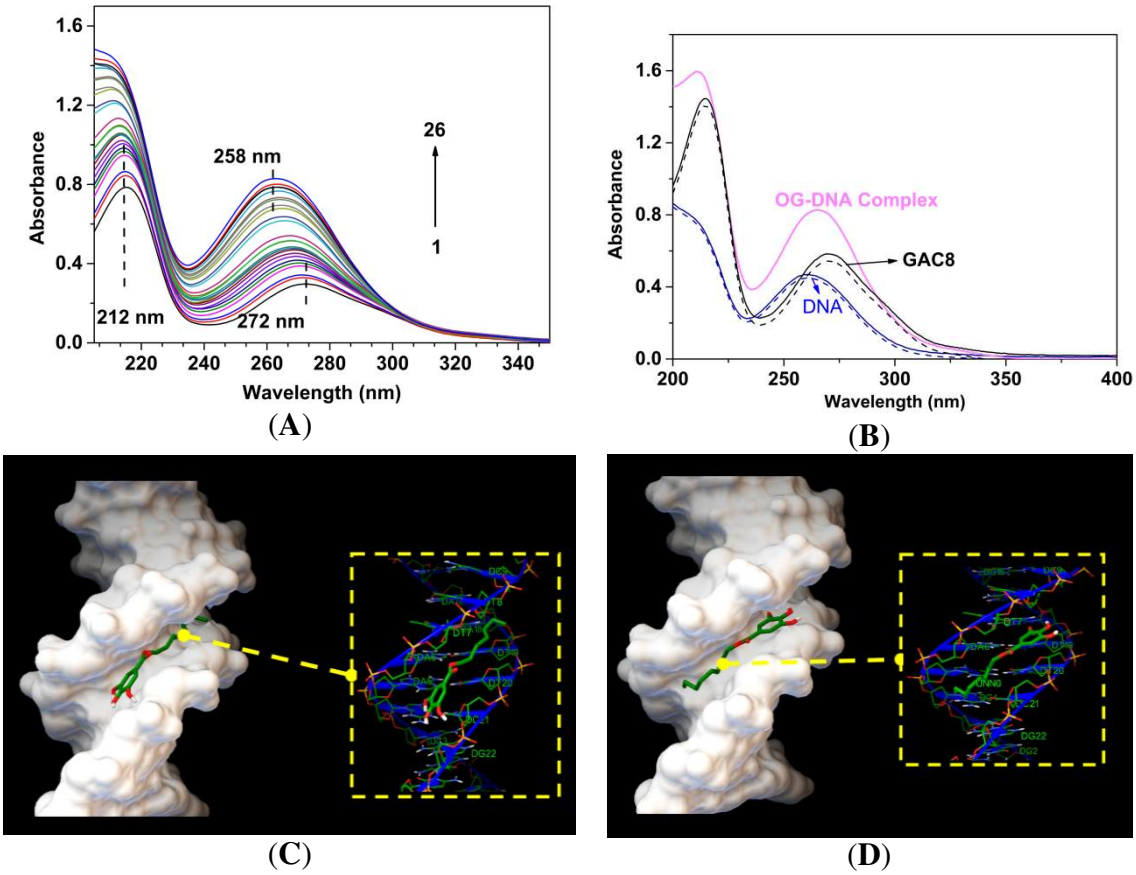

Fig. 4. (**A**) UV-vis spectra obtained from OG with increasing concentration of genomic DNA (**Experiment 1**), The initial concentration of OG was 5×10^{-5} M, while the concentration of DNA was 0, 0.29, 0.58, 0.87,..., 7.25×10^{-5} M for curves 1 to 26; (**B**) Recovered results by MCR-ALS. Molecular modeling posture of the DNA−OG system at (**C**) site 1 and (**D**) site 2. The area marked in green is hydrogen bonds.

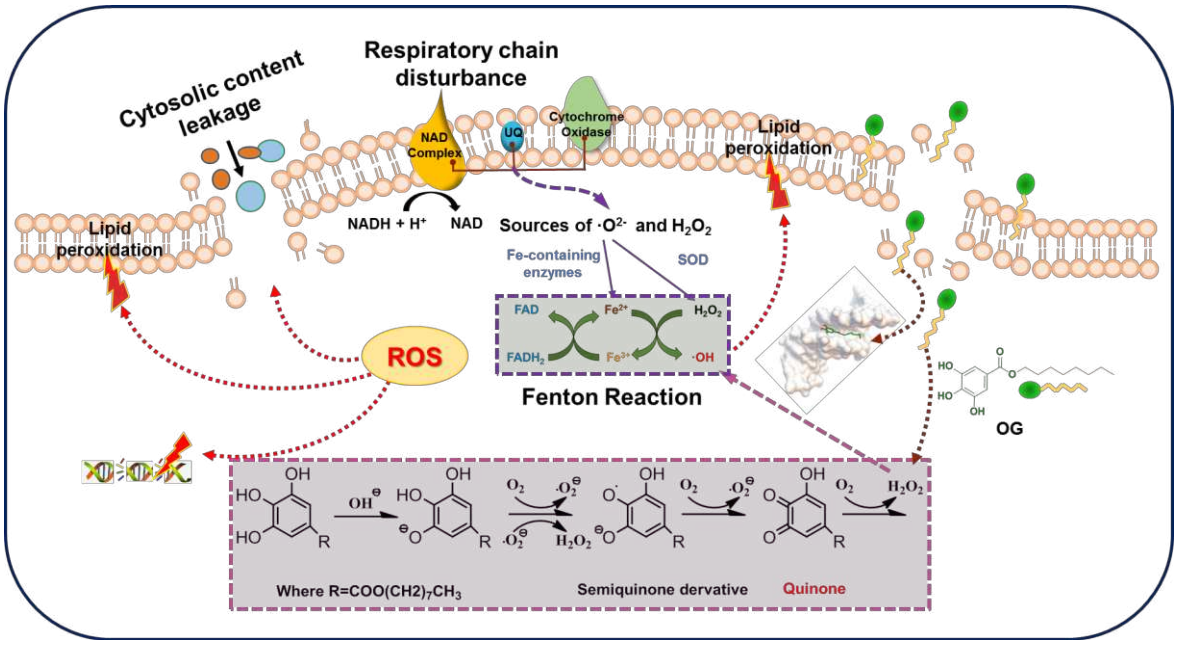
Cytosolic content leakage
Respiratory chain disturbance
NAD Complex
UQ
Cytochrome Oxidase
Lipid peroxidation
Lipid peroxidation
NADH + H+
NAD
Sources of ·O2- and H2O2
Fe-containing enzymes
SOD
FAD
Fe2+
H2O2
FADH2
Fe3+
·OH
ROS
Fenton Reaction
OG
Where R=COO(CH2)7CH3
Semiquinone dervative
Quinone

(A)

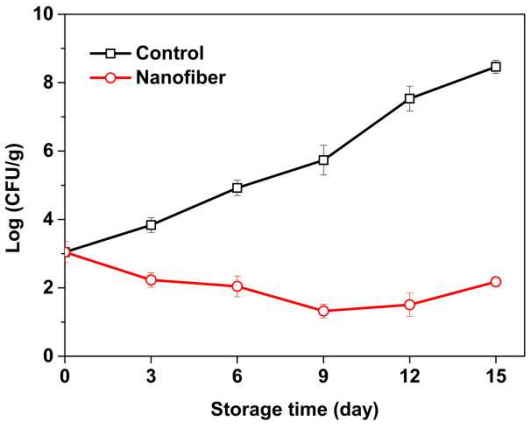
Control
Nanofiber
Log (CFU/g)
Storage time (day)

(B)

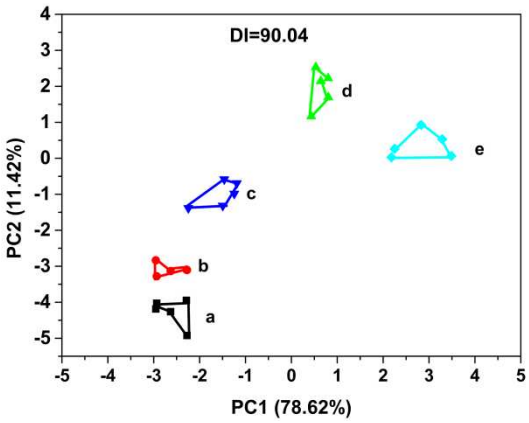
DI=90.04
a
b
c
d
e
PC2 (11.42%)
PC1 (78.62%)

(C)

858 **Fresh fish** **Treatment without NFs** **Treatment with NFs**

859 **(D)**

860 **Fig. 5**. Schematic mechanisms for the antibacterial activity of OG. (1) OG damages the membrane
861 of bacterial cells and easily permeates into the intact cells and then (2) interacts with DNA to
862 disturb the gene replication of bacteria. (3) OG disrupts the activity of ETC on the cytoplasmic
863 membrane to generate a high level of toxic ROS. The changes in preservation quality indices of
864 *Neosalanx taihuensis* Chen during storage at 4 ^{o}C. (**B**) Numbers of *E. coli* surviving on the
865 *Neosalanx taihuensis* Chen during storage at 4 ^{o}C. (**C**) PCA analysis of volatile odors of *Neosalanx*
866 *taihuensis* Chen. (a) fresh fish before the storage; Treatment with nanofiber for 6 days (b) and 15
867 days (c); Treatment without nanofiber for 6 days (d) and 15 days (e). (**D**) The appearance of the
868 packed *Neosalanx taihuensis* Chen in the absence and presence of electrospun nanofibers (CNFs)
869 containing OG during 15 days of storage at 4 ^{o}C.

870

Submit online to *Food Chemistry*

Antimicrobial mechanism of non-antibiotic lipophilic gallic acid derivatives against *Escherichia coli* and *Staphylococcus aureus* and its combined effect with electrospun nanofibers on Chinese Taihu icefish (*Neosalanx taihuensis* Chen) preservation

Yu-gang Shi*[a, b], Run-run Zhang [a], Chen-min Zhu [a], Ming-feng Xu [c], Qing Gu [a, b], Rammile Ettelaie [d], Shan Lin [a], Yi-fan Wang [a], Xin-yi Leng [a]

[a]*School of Food Science and Biotechnology, Zhejiang Gongshang University, Hangzhou, Zhejiang 310035, China*
[b]*Key Laboratory for Food Microbial Technology of Zhejiang Province, Zhejiang Gongshang University, Hangzhou, Zhejiang 310035, China*
[c] *Key Laboratory for Quality and Safety of Agricultural Products of Hangzhou ,College of Life and Environmental Sciences, Hangzhou Normal University, Hangzhou 311121, China*
[d]*School of Food Science and Nutrition, University of Leeds, Leeds, LS2 9JT, UK*

Corresponding Author:

Yu-gang Shi
School of Food Science and Biotechnology, Zhejiang Gongshang University, Xiasha University Town, Xuezheng Str. 18, Hangzhou 310018, China
Tel.: 86–0571–28008927
Email: yugangshi@zjgsu.edu.cn

SUPPORTING INFORMATION

1. Methods

1.1. Biocatalysis for preparation of alkyl gallates

The biocatalysis was carried out according to our previously published paper (Shi et al., 2017; 2018) with some modifications. Briefly, the alcoholysis reactions of MG with various fatty alcohols (1-butanol, 1-hexanol, 1-octanol, 1-decanol, 1-laurinol and 1-tetradecanol) was performed in a 30-mL glass vial using a screw-cap. MG and these aliphatic alcohols (1:6, molar ratio) were added to 10 mL of DES with water (10%, w/w). Experiments were conducted under sonochemical irradiation of 150 W, at 50 °C, for 1 h, after the addition of the lipase (CalB immo Plus, 10 mg, from Purolite Corporation, Hangzhou, China). And then the reaction vials were incubated at 60 °C, 200 rpm for 5-10 days. The supernatants were moved onto the TLC plate and HPLC equipped with a binary pump (G1312B) and Welchrom-C18 column (250 mm × 4.6 mm, 5 μm, Welch Materials, MD, U.S.A.). A sample of 50 μL taken out from the reaction medium was diluted with methanol of 800 mL and the internal standard of 50 mL was added to the mixture. The separation was carried out at 25 ^{o}C at 0.7 mL/min. The isocratic elution was conducted for 22 min using a mobile phase of 30A:70B (A: acetonitrile/water (70:30, v/v), B: 0.1% o-phosphoric acid). Evaporation of the solvent gave a product mixture, which was separated by silica gel column with the eluent of hexane/EA (96:4, v/v) /or crystallization. The structures of them were characterized by ^{1}H NMR and ^{13}C NMR.

1.2. Minimum inhibitory concentration (MIC) and Minimum bactericide concentration (MBC)

To determine the values of MIC and MBC, the assay was conducted according to our previously published paper (Shi et al., 2019) with slight modifications. In brief, the alkyl gallates stocks were prepared as described earlier and serially diluted in LB medium to final concentration (from 6.4 to 0.1 mM). The bacterial culture incubated overnight was diluted to approximately 10^{6} CFU mL^{-1} in LB, and they were added into all the tubes. The tube without gallates was considered as a negative control. All tubes were incubated for 24 h at 37 °C and a 1mL aliquot of the cultures treated with different concentrations of gallates was decimally diluted in 0.85% (w/v) NaCl solution, and spread-plated on LBA. The numbers of colonies were counted following 24 h incubation at 37 ^{o}C. The MIC was defined as the lowest concentration of alkyl gallates that inhibited visible growth of the bacteria in comparison with the control after 24 h. Concentrations, where ≤1 colony grew were

58 considered the MBC. The volume of ethanol corresponding to the highest dose of alkyl gallates
59 tested (1% ethanol final concentration) was used as a positive control and was found inactive.
60 Experiments were conducted in independent triplicate (n=3).

61 *1.3. Growth curve and time-kill kinetics analysis*

62 Both the growth curve assay and the time-kill kinetics analysis were performed according to our
63 previously published paper (Shi et al., 2019). The bacterial culture was incubated in the LB broth to
64 exponential phase at 37 ^{o}C for about 16 h and then diluted its final concentration to 10^6 CFU mL^{-1}.
65 The LB broth containing bacterial suspension and OG was added to each well to obtain the final
66 concentrations of 1×MIC, 2×MIC and 4×MIC and samples without the OG were set as the negative
67 control, then 200 μL mentioned culture was added into each well on 96-well microtiter plates. The
68 bacteria were further cultured at 37 ^{o}C, and cell growth was monitored at 600 nm using a hybrid
69 multi-mode microplate reader (Synergy H1, Biotek). As for the time-kill kinetics analysis, cultures
70 of bacteria at a concentration of 10^6 CFU mL^{-1} were exposed to various concentrations of OG broth
71 dilutions and cultures without OG set as a negative control. The mentioned solution was further
72 cultured at 37 °C at 180 rpm. After each selected incubation time point, aliquots (1 mL) were
73 transferred to another tube and decimally diluted in 0.85% sterile saline (w/v) and observed on LB
74 solid medium at 37 °C for about 18 h. The time-kill kinetics curves were drawn according to
75 plotting the value of Log CFU mL^{-1} versus time. To examine if the bactericidal effect of octyl
76 gallate could be attributed to hydroxy radicals (•OH), thiourea (150 mM) and DMSO (0.7 M) was
77 added simultaneously with octyl gallate. For the iron chelation experiments, 2,2'-dipyridyl (100
78 mM) was added simultaneously with octyl gallate.
79

80 *1.4. Propidium Iodide Uptake Test*

81 The propidium iodide (PI) uptake test was conducted according to the method described by Park
82 and Kang (2013) with some modifications to evaluate the cell membrane integrity. After inoculation,
83 all the solutions were incubated at 37 ^{o}C under 180 rpm agitation for 24 h. A 5 mL portion from
84 each tube was removed and then centrifuged at 6000 g at 4 °C for 15 min. Cell pellets were washed
85 ×3 with PBS (0.1 mM, pH 7.2) and then resuspended in the same buffer (10 mL) with the final cells
86 concentration of 10^6 CFU mL^{-1}. The alkyl ferulate ester was added at the final concentration of
87 1×MIC and then incubated at 37 ^{o}C under shaking conditions at 180 rpm for 4 h. A PI stock solution
88 of 1 mg mL^{-1} was prepared. After the alkyl ferulate ester treatment, cells were incubated with PI in
89 the dark at 37 ^{o}C for 10 min. For evaluation of PI uptake, fluorescence was monitored in a

fluorimeter (RF-5301PC, Shimadzu, Japan) using an excitation wavelength of 495 nm and an emission wavelength of 500-700 nm. Both slit widths were kept at 5-nm. The parallel sample without the alkyl ferulate ester was used as the negative control.

1.5. Cell Constituents' Release

The release of cell constituents into the supernatant was measured according to the method described by Lv et al., (2011) and Diao et al., (2014) with some modifications. Cells were collected by centrifugation at 5000 g for 10 min, washed ×3 with PBS (0.1 mM, pH 7.2), and resuspended in the same buffer. 5 mL of cell suspension were incubated at 37 ^{o}C under agitation in the presence of the OG. Then, 2 mL of each sample was centrifuged at 10,000 g for 5 min. Control groups containing bacterial supernatant without the alkyl ferulate ester treatments were tested similarly. The concentrations of proteins in supernatants were determined by Bradford assay. The amounts of DNA and RNA released from the cytoplasm into the supernatant were estimated by the detection of absorbance at 260 nm.

1.6. Evaluation of electrical conductivity

The electrical conductivity of the bacterial suspensions was determined as reported by Borges et al., (2013) with some modifications. Various bacteria were incubated overnight in TSB at 37 ^{o}C 180 rpm. The cells were harvested with centrifugation at 6000 g for 10 min and washed twice with sterile distilled water. The cell suspensions were adjusted to $OD_{640\ nm}$ = 0.2± 0.02. A volume of 1.8 mL of this culture was added to 200 uL of test compound (to a final concentration of 0.1 mM) and incubated for 1-8 h at 30 ^{o}C and 120 rpm. A negative control was prepared with sterile distilled water. The electrical conductivity of the bacterial suspensions was measured using a Nano Zetasizer (Malvern Instruments) equipment at room temperature.

1.7. Fatty acid methyl ester (FAME) analysis

FAME analysis was performed with an Agilent Agilent GC 7890B coupled with MS 5977B. The GC injection port was held at 250 °C with an injection volume of 1 μL in the splitless mode. A capillary column (HP-5 ms, 30 m × 0.25 mm × 0.25 μm; Agilent Technologies, U.S.A.) was used for the separation of FAMEs at a constant flow rate of 1 mL min^{-1}. The column oven temperature was programmed as follows: initiated at 30 °C; 30 °C min^{-1} to 200 ^{o}C; 5 °C min^{-1} to 215 °C; 1 °C min^{-1} to 220 °C, and held for 2 min; 10 °C min^{-1} to 280 °C, and held for 6 min. The mass

121 spectrometry conditions were set as follows: temperature of the ion source 240 °C; ionization mode
122 electron ionization (EI); ionization energy 70 eV. FAMEs were identified by their authentic
123 standards (AccuStandard, New Haven, CT, U.S.A.) and comparison with standard mass spectra in
124 Mass Spectral Library provided by the National Institute of Standards and Technology
125 (Gaithersburg, MD, U.S.A.) (NIST05). The relative amounts of fatty acids were quantified from the
126 peak areas of the corresponding FAMEs using Agilent ChemStation as described in the previous
127 study.
128

129 *1.8. Scanning electron microscopy (SEM) analysis*

130 To determine the efficacy of OG and the morphological changes of bacteria, SEM studies were
131 conducted according to our previously published paper (Shi et al., 2018). After treatment of OG, the
132 bacteria were obtained with centrifugation at 6000×g for 10 min and washed with the mentioned
133 PBS three times and then added to 1 mL 2.5% (v/v) glutaraldehyde, save overnight at 4 ^{o}C. Then
134 postfixed with 1% OsO4 in phosphate buffer for 1-2h and washed three times in the phosphate
135 buffer(0.1 M，pH7.0) for 15min at each step. The sample is dehydrated with a gradient of ethanol,
136 then dehydrated in Hitachi Model HCP-2 critical point dryer. The dehydrated sample was coated
137 with gold-palladium in Hitachi Model E-1010 ion sputter for 4-5min and observed in Hitachi Model
138 SU-8010 SEM.
139

140 *1.9. UV-vis spectral data matrix and chemometrics methods*

141 Two different titration experiments were performed to get the expanding UV-vis spectral data
142 matrix. Experiment A: the concentration of OG was kept at 0.05 mM, and different concentrations
143 of genomic DNA solution (0 to 24.25 μg/mL, a total of 26 samples) were titrated into the OG
144 solution. Experiment B: the concentration of the genomic DNA solution was fixed at 12.17 μg/mL,
145 and different concentrations of OG (0 to 0.05 mM, a total of 26 samples) were added to the solution.
146 After each titration, the solution was mixed thoroughly and equilibrated for 10 min before the
147 spectroscopic was collected. All spectral changes of the OG or genomic DNA solution were
148 recorded and the UV-vis spectral data matrix was constructed using a Shimadzu UV-2600
149 spectrophotometer. The original spectroscopic data matrix was imported into Matlab, and then
150 treated by a chemometrics approach, namely multivariate curve resolution-alternating least squares
151 (MCR-ALS).
152

153 *1.10. Molecular docking*

154 The structure of OG was prepared with ChemBioDraw Ultra 12.0, and its 3D structure was
155 optimized using ChemBio3D Ultra 12.0 and exported as a pdb file. The crystal structure of DNA
156 (PDB ID: 1N37) was downloaded, and the RSD17 residue was removed to obtain pure DNA.
157 Optimal DNA was obtained by removing all water molecules and adding polar hydrogen atoms and
158 Gasteiger charges with the support of AutoDockTools-1.5.6. AutoDock 4.2 software (The Scripps
159 Research Institute La Jolla, U.S.A.) was utilized to run docking programs with the Lamarckian
160 Genetic Algorithm as the docking parameters algorithm.
161

162 *1.11. NAD^+/NADH ratio test.*

163 The Sigma-Aldrich analysis kit (MAK037) was used to evaluate the NAD^+/NADH ratio of bacterial
164 cells. The cells were washed with cold PBS (0.1 M, pH 7.2) and centrifuged at 2000 g for 5 minutes.
165 Cells were extracted with 400 μL of NAD^+/NADH extraction buffer by homogenization or
166 freezing/thawing for two cycles of 20 minutes on dry ice followed by 10 minutes at room
167 temperature. To remove insoluble, the sample was vortexed for 10 seconds and then centrifuged at
168 13000 g for 10 minutes. The extracted NAD^+/NADH supernatant was transferred to labeled test
169 tubes. The supernatant was then used for NAD^+/NADH determination. To detection of total NADH
170 and NAD, transfer up to 50 μL of the extracted sample in duplicate into a 96 well plate. Bring
171 samples to a final volume of 50 μL with NADH/NAD extraction buffer. To detection of NADH,
172 NAD must be decomposed before the reaction. Decompose NAD by aliquoting 200 μL of extracted
173 samples into microcentrifuge tubes and heat to 60 ^{o}C for 30 minutes in a water bath or a heating
174 block. Add 100 μL of the Master Reaction Mix to each of the wells. Mix well using the horizontal
175 shaker or by pipetting and incubate the reaction for 5 minutes at room temperature to convert NAD^+
176 to NADH. Add 10 μL of NADH Developer into each well. Incubate at room temperature for 4 hours.
177 Measure the absorbance at 450 nm (A450).
178

179 *1.12. MDA generation in E. coli*

180 The content of MDA was determined by the kit (Abcam). The principle is that MDA can react with
181 TBA at a higher temperature and in an acidic environment to form a red MDA-TBA adduct, which
182 has a maximum absorption at 535 nm. The bacteria were harvested and washed with cold PBS (0.1
183 M, pH 7.2) after exposure to OG (0.1, 0.2, 0.4 mM) for 2 hours. Then, the cells were homogenized

184 in MDA lysis buffer and centrifuged at 13000 g for 10 minutes. The supernatant was collected for
185 MDA measurement. The supernatant and TBA working solution were mixed and heated in boiling
186 water for 15 minutes. Cool to room temperature, centrifuge at 1200 g for 10 minutes, and add 200
187 μL of supernatant to a 96-well plate. The MDA production level of each experimental group was
188 quantified according to the specific absorption rate at 535 nm (Porter, 2013).
189

190 *1.13. Genome integrity determination*

191 *E. coli* was cultured to the plateau phase, diluted to 10^6 CFU mL^{-1} in LB. Then, cells with the
192 treatment of OG at 1×MIC served as the experimental groups, whereas cells without the treatment
193 of OG served as the control groups. After co-cultivation for 12 h, 3 mL of bacterial solution was
194 collected by centrifugation (6000 g, 4 ^{o}C, of 5 mins) to extract genomic DNA according to the
195 bacterial DNA extraction kit (Sangon, Shanghai). Mix the extracted DNA sample with the DNA
196 Loading Buffer (*V*/*V*=1:1) to the electrophoresis gel. Set the parameters of the DNA electrophoresis
197 instrument to a voltage of 100 V and a time of 30 mins. Finally, observe and record the
198 electrophoresis through the gel imager.
199
200

201 *1.14. For Q-PCR analysis*

202 *RNA Extraction and cDNA Synthesis.*
203 Bacteria were incubated 2 h in the presence or absence of the OG, at 37 °C with constant agitation.
204 For gene expression analysis, *E. coli* cells were grown in LB at a high density, 1×10^9 CFUs in a
205 final volume of 1 mL for each RNA extraction. The total RNA was isolated from *E. coli* using
206 Bacteria Total RNA Isolation Kit (Sangon Biotech). The concentration and purity of the RNA were
207 determined by measuring OD260 nm and OD280 nm using a Nanodrop2000 Ultraviolet
208 Spectrophotometer (Thermo Fisher, MA, USA). For cDNA synthesis, 500 ng of total RNAs were
209 reverse-transcribed using Hifair II 1st strand cDNA Synthesis SuperMix Kit (Hifair) and stored at
210 -20 ^{o}C.
211

212 *RNA extraction and real-time quantitative PCR analysis*
213 Hifair qPCR SYBR Green Master Mix kit (Hifair) and IQ5 Thermocycler (Bio-Rad) were used. As
214 an internal standard, gene ssrA was used, which encodes for 16S ribosomal RNA. All PCR
215 reactions were carried out in a final volume of 20 μL, using 10 μL of Hifair qPCR SYBR Green

216 Master Mix, 2 μL of reverse-transcription reaction (approximately 2-5 ng of total cDNA) and 0.2
217 μM of each primer (Table 1S).
218
219 For the more expressed 16S rRNA, amplification was carried out with 1 μL of 1000-fold diluted
220 reverse-transcription reaction. Negative controls were included for each specific PCR reaction,
221 consisting of the amplification mixture without the cDNA. The amplification conditions were as
222 follows: 1 cycle at 95 °C for 5 min, 95 °C for 10 s, 40 cycles at 60 °C for 10 s and 72 °C for 20 s.
223 To ensure the specificity of the PCR products, melting curve analysis was performed by heating
224 products to 95 °C for 15 s, followed by cooling to 60 °C and slowly heating to 95 °C while
225 monitoring fluorescence. Data collection and analysis were carried out by the use of IQ5 Optical
226 System software (version 2.1, Bio-Rad). Data were normalized to levels of ssrA and analyzed by the
227 use of the comparative critical threshold method for calculation of the ΔΔCt and Expression Fold
228 (EF = $2^{-\Delta\Delta Ct}$) between the treated and untreated samples. The values of EF were reported as the
229 average ± standard deviations of three independent experiments, each conducted in triplicate.
230 Statistical significance was calculated with Student's t-test, and a $P<0.05$ was considered
231 significant.
232
233
234 **Table S1**
235 List of primers used for the quantivitative RT-PCR

Gene name	Primer sequence
sodA	Forward: GCCTGTTCTGGAAAGGTCTG Reverse: CCAGTTTATCGCCTTTCAGC
soxR	Forward: GTATCCGTAACAGCGGCAAT Reverse: CATTGGGACGAAAGCTGTTT
soxS	Forward: TTATCGCATGGATTGACGAG Reverse: ACATAACCCAGGTCCATTGC
oxyR	Forward:CATTCATTGAAGTGCCGTTG Reverse: CGCGGAAGTGTGTATCTTCA
ahpC	Forward: AAACCAGGCATTCAAAAACG Reverse: TGCTTTGTGGGTGAAGTGAG
oxyS	Forward: GGAGCGGCACCTCTTTTAAC Reverse: ATCCTGGAGATCCGCAAAAG
dps	Forward: CAAAACCCCGCTGAAAAGTTAC

	Reverse: GATATCTGCGGTGTCGTCATCT
gorA	Forward: GATGTATACCGCCGTCACCA Reverse: AGCCCTGCAACATTTCGTC
katG	Forward: CTGGTGTGGTTGGTGTTGAG Reverse: AGTGACTCGGTGGTGGAAAC
ahpF	Forward: CCGCAGGGTATCATCCAG Reverse: TTAGCCGGGCAAACTTCA
ssrA	Forward: TTAGGACGGGGATCAAGAGA Reverse: GCGTCCGAAATTCCTACATC

1.15. Preparation of electrospinning solutions and nanofibers (NFs)

The solutions for electrospinning and NFs were prepared using the method described by Liu et al. (2018) with a slight modification. Briefly, the solutions used for electrospinning were obtained by dissolving poly(lactic acid) (PLA) in hexafluoroisopropanol (HFIP) (9%, *w*/*v*, 0.9 g of PLA in 10 mL HFIP) at room temperature under stirring for 3 h. The OG/*β*-cyclodextrin inclusion complexes (OG/*β*CD, 6%, *w*/*v*) were added into the solution with magnetically stirring for 12 h at room temperature to obtain the homogeneous solution for electrospinning. The prepared solution was put into a 10 mL plastic syringe fitted with a 23G (outer/inner diameter; 0.64 mm/0.33 mm) metallic needle. The solution flow rate was 1 mL h^{-1}. The loaded syringe was fixed horizontally with a syringe pump (Baoding longer, LSP03-1A) and the electrode of the high voltage power supply (Tianjin Dongwen, DWLP303-1ACDB) was connected to the metal needle tip. The working distance between the needle tip and the ground electrode was 15 cm. The electrospinning voltage was 18 kV. The electrospinning temperature and the relative humidities were 25 ^{o}C and 45%, respectively. The collected fibers were vacuum dried for 24 h to remove solvent residue and used for the analysis of its morphology via scanning electron microscopy (SU8010, Hitachi, Japan) (see Fig. S1) and the preservation of icefish (Fig. 5D).

The morphological analysis of the composite electrospinning nanofibers containing OG was carried out using Hitachi T-1000 scanning electron microscope (Hitachi High-Technologies Corporation, Tokyo, Japan), with an acceleration voltage of 15 kV, as shown in Fig. S1. The composite nanofibers were set on a metallic stub and covered with gold under vacuum in an argon atmosphere.

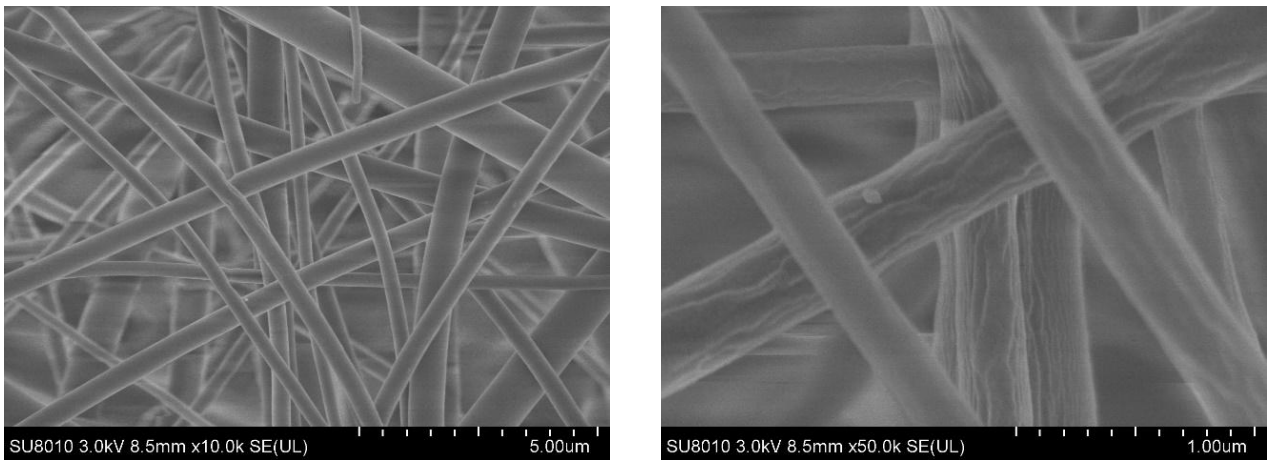

Fig. S1. SEM images PLA-OG/βCD nanofibers.

1.16. The electronic nose

The electronic nose (Fig. S2) applied in the experiment was also developed by us. It consists of a sampling system, a detector containing the array of sensors, and pattern recognition for data recording. The sensor array is composed of fourteen different metal oxide sensors. Each sensor has a certain degree of affinity toward specific chemicals or volatile compounds. The sensors' response to changes in conductivity induced by the adsorption of gas-phase molecules and on subsequent surface reactions. Before the measurement, the system of the electronic nose was cleaned with zero-air which was indoor air-filtered by active carbon. The main purpose of zero-air was to clean the circuit and to return the sensors to the baselines. During the measurement of icefish, the headspace gas of a sample was pumped into the sensor chamber at a constant rate of 0.6 L/min through a tube connected to a needle. The response of each sensor was expressed as a ratio of conductance (G/G0, G and G0 are conductances of the sensors' response to the sample gas and the zero-air, respectively). The measurement procedure was controlled by a special program. The measurement time was 160 s, which was sufficient for each sensor to reach a stable value. The cleaning time was set to 100 s. The data was stored after the measurement was completed. The same sample was paralleled 5 times.

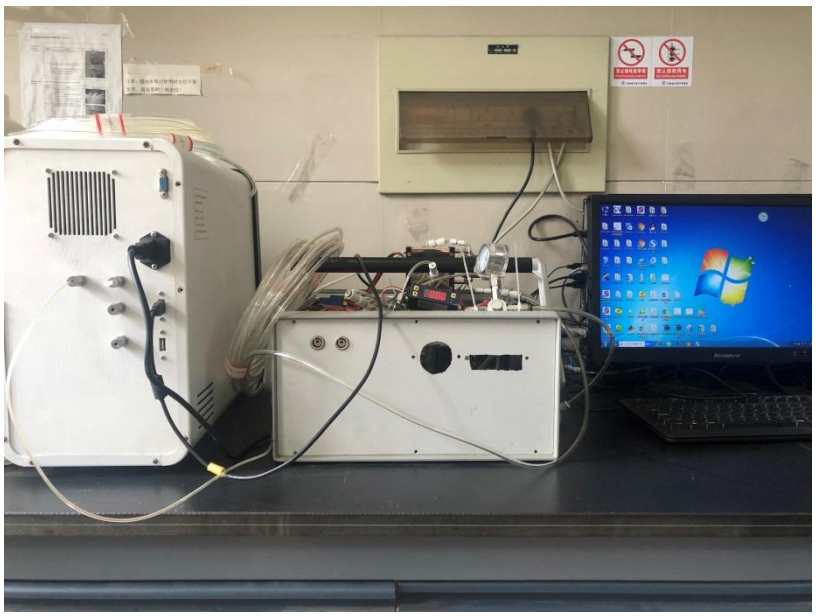

Fig. S2. The electronic nose

2. Results

Table S2. Membrane fatty acid composition of stationary stage cells of *E. coli* at different concentrations of OG.

Bacteria	Fatty acids	Total composition (%) at different concentrations of OG		
		0	0.025 mM	0.05 mM
	C12:0	1.51 ± 0.4	2.01 ± 0.12	2.23 ± 0.01
	C13:0	0.46 ± 0.18	0.37 ± 0.01	0.44 ± 0.05
	C14:0	3.47 ± 0.75	2.65 ± 082	1.78 ± 0.00
	C15:0	4.51± 0.00	3.78 ± 0.1	3.16 ± 0.06
	C16:1	4.45 ± 0.07	4.1 ± 0.02	4.59 ± 1.36
E. coli	C16:0	30.69 ± 0.24	24.99 ± 0.23	16.64 ±0.31
	C17cyclo	4.58 ± 0.01	1.51 ± 0.03	1.81 ± 0.82
	C17:0	3.46 ± 0.03	1.39 ± 0.15	1.13 ± 0.04
	C18:2	11.84 ± 0.94	14.49 ± 0.85	24.33 ± 1.93
	C18:1	5.53 ± 0.14	24.93 ± 1.57	28.79 ± 1.98
	C18:0	24.04 ± 1.97	15.18 ± 1.04	11.06 ± 1.04

	C19cyclo	5.15 ± 0.12	4.13 ± 0.42	3.06 ± 0.04
	C20:0	0.31 ± 0.01	0.47 ± 0.02	0.98 ± 0.06
	UFAs	21.82 ± 1.46	45.52 ± 2.48	57.71 ± 2.78
	SFAs	78.18 ± 3.26	56.48 ± 2.57	42.29 ± 2.15

289 Data represent the mean value ± SD (n=3). Different letters in the same group of bacteria means
290 significant differences (P< 0.05).
291
292 **Table S3.** Membrane fatty acid composition of stationary stage cells of *S. aureus* at different
293 concentrations of OG.

Bacteria	**Fatty acids**	**Total composition (%) at different concentrations of OG**		
		0	0.02 mM	0.033 mM
	C10:0	0.12 ± 0.01	0.11 ± 0.02	0.21 ± 0.01
	C12:0	4.61 ± 0.13	5.92 ± 0.09	8.14 ± 0.28
	isoC14:0	1.42 ± 0.05	0.91 ± 0.03	0.53 ± 0.09
	anteisoC14:0	2.77 ± 0.07	1.58 ± 0.09	1.53 ± 0.14
	C14:0	3.83 ± 0.29	3.52 ± 0.27	3.42 ± 0.09
	isoC15:0	7.34 ± 0.03	4.15 ± 0.09	3.64 ± 0.07
	anteisoC15:0	22.56 ± 0.12	17.58 ± 0.09	14.74 ± 0.24
S. aureus	C16:0	14.55 ± 0.03	19.53 ± 0.62	23.97 ± 1.06
	isoC17:0	4.97 ± 0.09	5.36 ± 0.67	5.74 ± 0.12
	anteisoC17:0	7.91 ± 0.37	4.86 ± 0.19	3.3 ± 0.04
	C18:1	3.15 ± 0.26	2.57 ± 0.44	2.03 ± 0.07
	C18:0	14.25 ± 0.76	17.25 ± 0.63	20.16 ± 0.86
	C19:0	2.09 ± 0.08	2.41 ± 0.01	2.64 ± 0.03
	C20:0	6.25 ± 0.21	7.09 ± 0.02	7.36 ± 0.23
	UBFAs	48.85 ± 3.14	58.4 ± 4.28	67.84 ± 5.09
	BCFAs	51.15 ± 2,14	41.6 ± 2.09	32.16 ± 1.07

294 Data represent the mean value ± SD (n=3). Different letters in the same group of bacteria means
295 significant differences (P< 0.05).
296

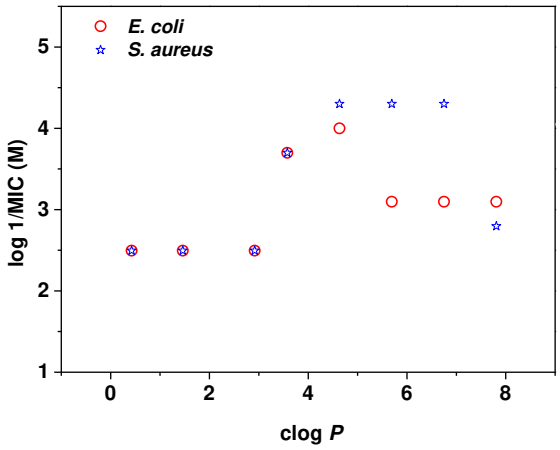

297

298 **Fig. S3.** Correlation between the antimicrobial activity of GA and GAEs against *E. coli* and *S.*
299 *aureus* and clog*P*.

300

301

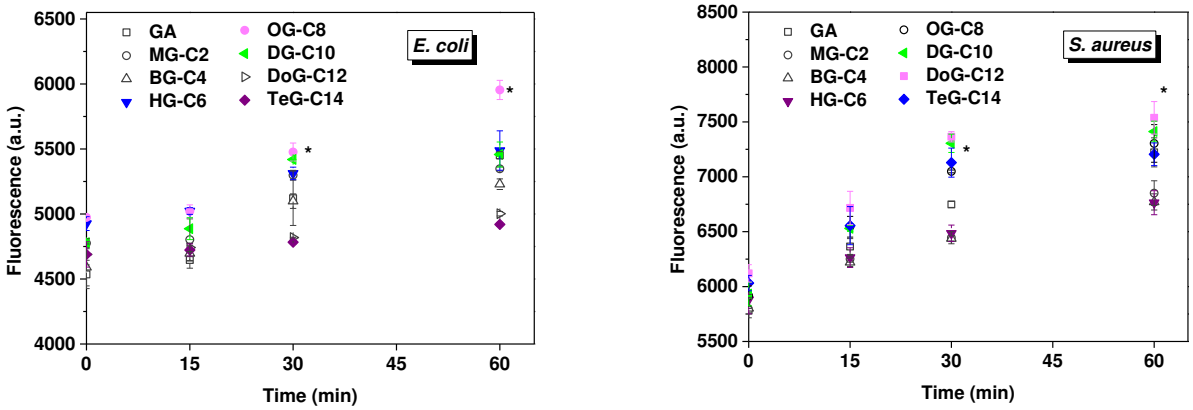

302

303 **Fig. S4.** The uptake of OG in *E. coli*. After each gallate (0.06 mM) was mixed with *E. coli* and *S.*
304 *aureus* cells (10^8 CFU mL^{-1}), the suspension was vortexed and then absorbance at 272 nm of the
305 supernatant obtained by centrifugation for 2 min was measured. **P*<0.05 (vs the groups treated with
306 other alkyl gallates).

307

308

309

310

311

312

313

314

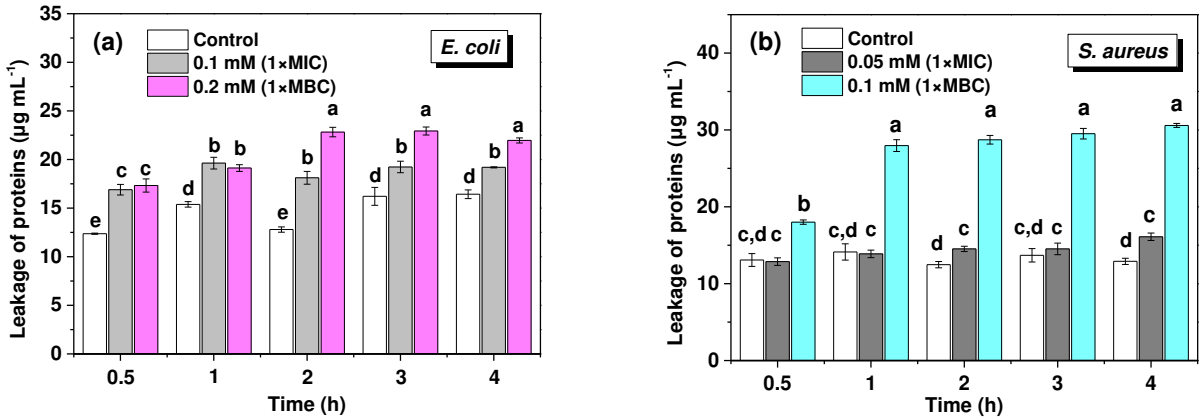

315 **Fig. S5.** The leakage of both UV-absorbing substances ($OD_{260\ nm}$) and proteins of bacteria treated
316 without or with OG (1×MIC and 1×MBC) for 0.5 h, 1 h, 2 h and 4 h. (**a3**) for *E. coli* and (**b3**) for *S.*
317 *aureus*.

318

319

320

321

322

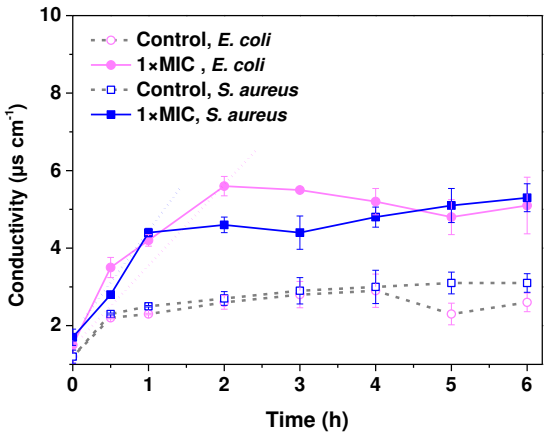

323

324 **Fig. S6.** Surface zeta potential of *E. coli* and *S. aureus.* Data represent the mean value ± SD (n = 3).
325 Different letters in the same group of bacteria mean significant differences ($P < 0.05$).

326

327

328

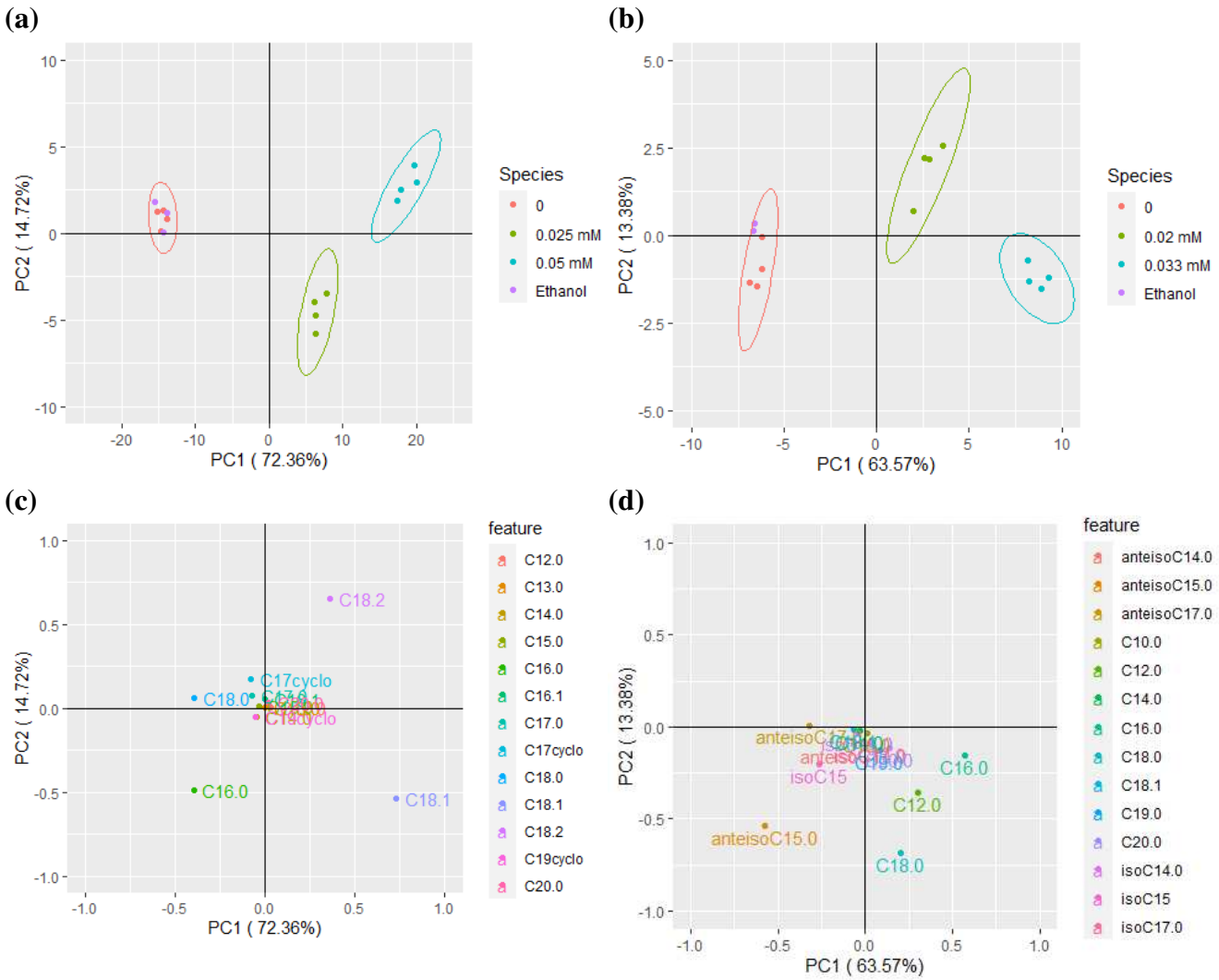

Fig. S7. Principal component analysis of MFAs composition of *E. coli* and *S. aureus* cells. Scores plot of fatty-acid composition of (**a**) *E. coli* and (**b**) *S. aureus* using the first two principal component analysis in relation to ethanol (1 %) and different concentrations of OG. Loadings plot of fatty-acid composition of (**c**) *E. coli* and (**d**) *S. aureus* in different concentrations of OG defined by the first two principal components.

A total of 13 fatty acids in the *E. coli* cell membrane and a total of 14 fatty acids in the *S. aureus* cell membrane were identified by GC−MS. To investigate which fatty acids were mainly responsible for discrimination between the control and samples treated with OG, the GC−MS data were processed by using an unsupervised clustering method, PCA analysis. The scores plot was generated to show the clustering of cell-membrane samples according to their fatty-acid

composition, while the corresponding loading plot was produced to identify fatty acids that had a significant influence on the separation or clustering of data. As for *E. coli*, the first two principal components accounted for 87.08% of the total variance in the *E. coli* cell membrane, distributed between PC1 (72.36%) and PC2 (14.72%) positions (Fig. S7-a). Distinct clustering was found in different groups except for the control and ethanol groups, suggesting that the exposure of *E. coli* cells to OG may lead to systematic changes in the membrane fatty-acid composition of *E. coli*, while ethanol (1%) had no significant effect on them compared to the control. In the PCA model, the contribution of each fatty acid to a specific component is reflected in the loading value in the loading plot. The fatty acids with the highest loading values account for the biggest differences among cells grown at different concentrations of OG. As shown in Fig. S7-c, two variables, namely oleic acid (C18:1) and linoleic acid (C18:2), had positive loading values on PC1, implying that their contents were considerably high in the membrane of OG-treated groups. In contrast, hexadecanoic acid (C16:0) was on the negative side of both PC1 and PC2, which may reflect a low content in *E. coli* cells exposed to OG at the highest concentration (0.05 mM). Stearic acid (C18:0) was distributed on the positive side of PC2, which may be due to a high proportion of this kind of fatty acid in the cell membrane of *E. coli* cultivated with OG. These four fatty acids were correlated in the PC1 or PC2 space, suggesting that they were the best markers for differentiating OG-treated cells from the control.

Likewise, for *S. aureus*, the first two principal components accounted for 76.95% of the total variance, distributed between PC1 (63.57%) and PC2 (13.38%) positions. Distinct clustering was also found in different groups except for the control and ethanol group (Fig. S7-b). Three variables, namely dodecanoic acid (C12:0), palmitic acid (C16:0) and octadecanoic acid (C18:0), had positive loading values on PC1 (Fig. S7-d), implying that their contents in the cell membrane were considerably high after *S. aureus* was incubated in the presence of OG. In contrast, anteisopentadecanic acid (anteisoC15:0), isopentadecanic acid (isoC15:0) were on the negative side of both PC1 and PC2, which may reflect a low content in *S. aureus* cells exposed to OG at the highest concentration (0.02 mM). Anteisoheptadecanoic acid (anteisoC17:0) was distributed on the positive side of PC2. This observation maybe because there was a high proportion of this kind of fatty acid in the cell membrane of *S. aureus* cultivated in the absence of OG. These five fatty acids were correlated in the PC1 or PC2 space, suggesting that they were the best markers for differentiating OG-treated cells from the control.

379

380

(a) **(b)**

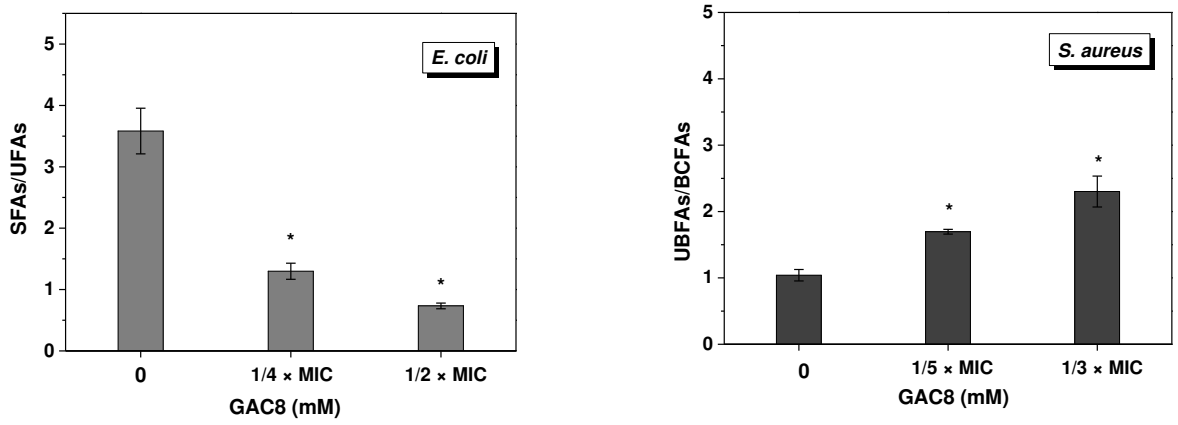

381

382

383 **Fig. S8.** (**a**) ratios of SFAs to UFAs in the cytoplasmic membrane of *E. coli* grown with different
384 concentrations of OG. (**b**) ratios of UBFAs to BCFAs in the cytoplasmic membrane of *S. aureus*
385 grown with different concentrations of OG, respectively. Data represent the mean value ± SD (n=3).
386 The superscript (*) indicates significantly different to equivalent control points (P<0.05).

387

388

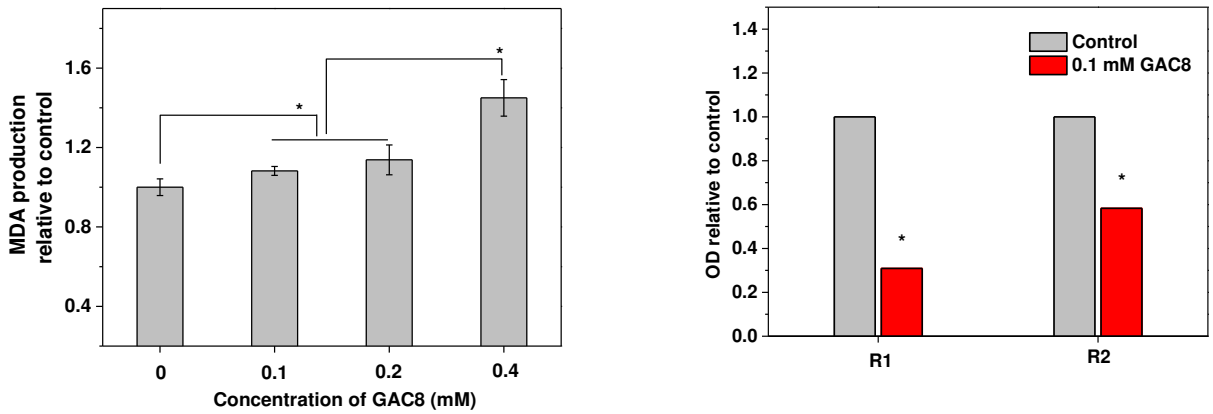

(**A**) (**B**)

389 **Fig. S9.** (**A**) Malondialdehyde in OG-treated *E. coli*. *P < 0.05. (**B**) The relative of integrated
390 optical density (IOD) value of the electrophoresis band. The superscript (*) indicates significantly
391 different to equivalent control points (P<0.05).

392

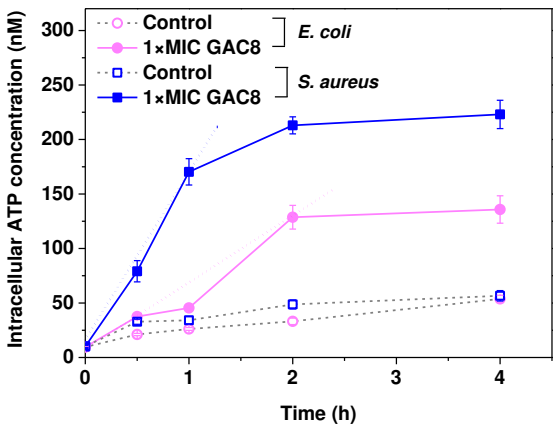

Fig. S10. Effect of OG on the intracellular ATP concentration in *E. coli* and *S. aureus*.

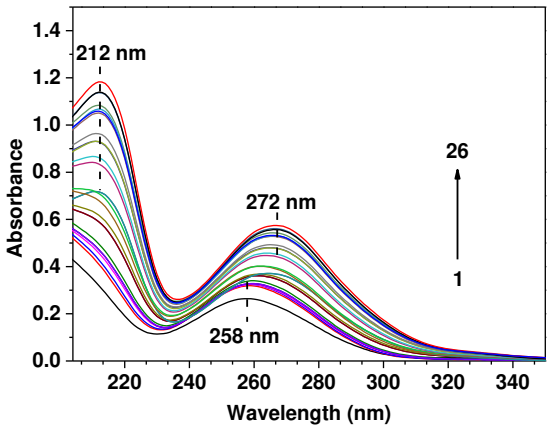

Fig. S11. Genomic DNA in the presence of OG (**Experiment 2**), c(DNA) = 3.7×10^{-5} M, the concentration of OG was 0, 0.3, 0.6, 0.9, 1.2..., 7.5×10^{-5} M for curves 1 to 26.

In Fig. S11, the spectrum of DNA was characterized by a peak at 258 nm, which strongly related to the absorption of purine and pyrimidine bases in DNA. The interaction of OG with DNA was monitored by the hypochromism and blue shifting of the band at 212 nm. The intensity of the peak significantly enhanced as OG was gradually added.

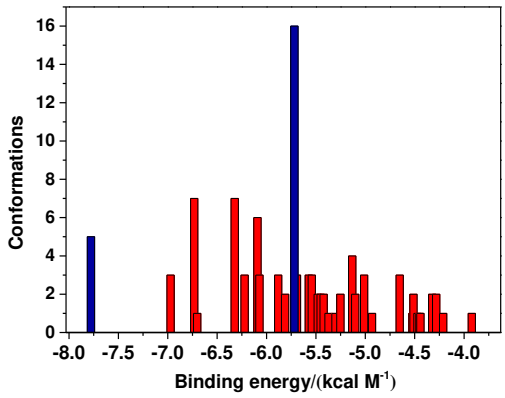

Fig. S12. Cluster analyses of the AutoDock docking 100 runs of OG with DNA (PDB: 453D).

In Fig. S12, 100 docking runs were conducted finally, 36 multimember conformational clusters were generated. Among them, the lowest energy cluster contained 5 of 100 conformations with an estimated binding energy of -7.8 kcal M^{-1}. The highest number cluster included 16 confirmations with a binding energy of -5.74 kcal M^{-1}. Ultimately those two binding models were chosen for binding-position analyses to interpret the molecular interaction mechanism of OG with DNA. OG was bound to A-T rich regions of DNA covered residues A5, A6, A7, T7, T19, T20 both in site 1 and site 2 which can be attributed to A-T regions have narrower space than G-C region and offer a better fit of small molecules into the minor groove like OG (Ketan Sahoo et al., 2008).

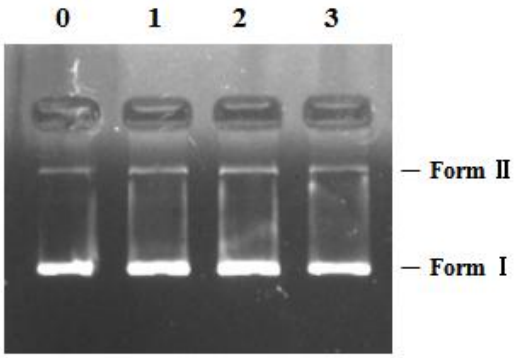

(**E**)

Fig. S13. Agarose gel electrophoresis of pBR322 plasmid DNA treated with different concentrations of OG. Lane 0: control; and lanes 1–3: 0.1, 0.2 and 0.4 mM of OG.

Agarose gel electrophoresis of free DNA and DNA exposed to OG was employed to access whether it had DNA cleavage ability. If one strand of circular plasmid DNA is cleaved, the supercoiled form (Form I) will relax to produce a slower-moving open circular form (Form II). If both strands are

428 cleaved, a linear form will be generated which migrates in between. As shown in Fig. S13, the
429 bands of plasmid pBR322 DNA treated with different concentrations of OG were similar to that of
430 control (lane 1), indicating that OG had no ability to cause DNA cleavage. These results imply that
431 the interaction of OG with DNA as the other antibacterial mechanisms may be involved as well.
432

433 **Reference**

434 Álvarez-ordóñez, A., Fernández, A., López, M., Arenas, R., & Bernardo, A. (2008). Modifications
435 in membrane fatty acid composition of *Salmonella typhimurium* in response to growth
436 conditions and their effect on heat resistance. *International Journal of Food Microbiology, 123,*
437 212-219.

438 Di Pasqua, R., Hoskins, N., Betts G., & Mauriello, G. (2006). Changes in membrane fatty acids
439 composition of microbial cells induced by addiction of thymol, carvacrol, limonene,
440 cinnamaldehyde, and eugenol in the growing media. *Journal of Agricultural & Food Chemistry,*
441 *54 (7),* 2745-2749.

442 Fatma, K., Umu, O. C. O., Tekinay, T., & Uyar, T. (2013). Antibacterial electrospun poly (lactic acid)
443 (PLA) nanofibrous webs incorporating triclosan/cyclodextrin inclusion complexes. *Journal of*
444 *Agricultural & Food Chemistry, 61 (16),* 3901-3908.

445 Kubo, I., Masuoka, N., Xiao, P., & Haraguchi, H. (2002). Antioxidant activity of dodecyl gallate.
446 *Journal of Agricultural & Food Chemistry, 50 (12),* 3533-3539.

447 Kubo, I., Xiao, P., & Fujita, K. (2001). Antifungal activity of octyl gallate: structural criteria and
448 mode of action. *Bioorganic & Medicinal chemistry letters, 11 (3),* 347-350.

449 Patrignani, F., Iucci, L., Belletti, N., Gardini, F., Guerzoni, M. E., & Lanciotti, R. (2008). Effects of
450 sub-lethal concentrations of hexanal and 2-(E)-hexenal on membrane fatty acid composition and
451 volatile compounds of *Listeria monocytogenes*, *Staphylococcus aureus*, *Salmonella enteritidis*
452 and *Escherichia coli*. *International Journal of Food Microbiology, 123,* 1-8.

453 Porter, N. A. (2013). A perspective on free radical autoxidation: the physical organic chemistry of
454 polyunsaturated fatty acid and sterol peroxidation. *Journal of Physical Organic Chemistry, 78*
455 *(8),* 3511-3524.

456 Sakihama Y, Cohen M F, Grace S C & Yamasaki, H. (2002). Plant phenolic antioxidant and
457 prooxidant activities: phenolics-induced oxidative damage mediated by metals in plants.
458 *Toxicology, 177 (1),* 67-80.

459 Siliakus, M. F., Oost, J. V. D., & Kengen, S. W. M. (2017). Adaptations of archaeal and bacterial
460 membranes to variations in temperature, pH and pressure. *Extremophiles, 21,* 651-670.

461Wang, X., Yang, P., Li, J., Ihsan, A., Liu, Q., Cheng, G., ... Yuan, Z. (2016). Genotoxic risk of
462 quinocetone and its possible mechanism in vitro studies. *Toxicology Research, 5 (2),* 446-460.

Declaration of interest statement

We declare that we have no financial and personal relationships with other people or organizations that can inappropriately influence our work, there is no professional or other personal interest of any nature or kind in any product, service and/or company that could be construed as influencing the position presented in, or the review of, the manuscript entitled.